NASA
Technical
Paper
3146

December 1991

HZETRN: A Heavy Ion/Nucleon Transport Code for Space Radiations

John W. Wilson,
Sang Y. Chun,
Forooz F. Badavi,
Lawrence W. Townsend,
and Stanley L. Lamkin

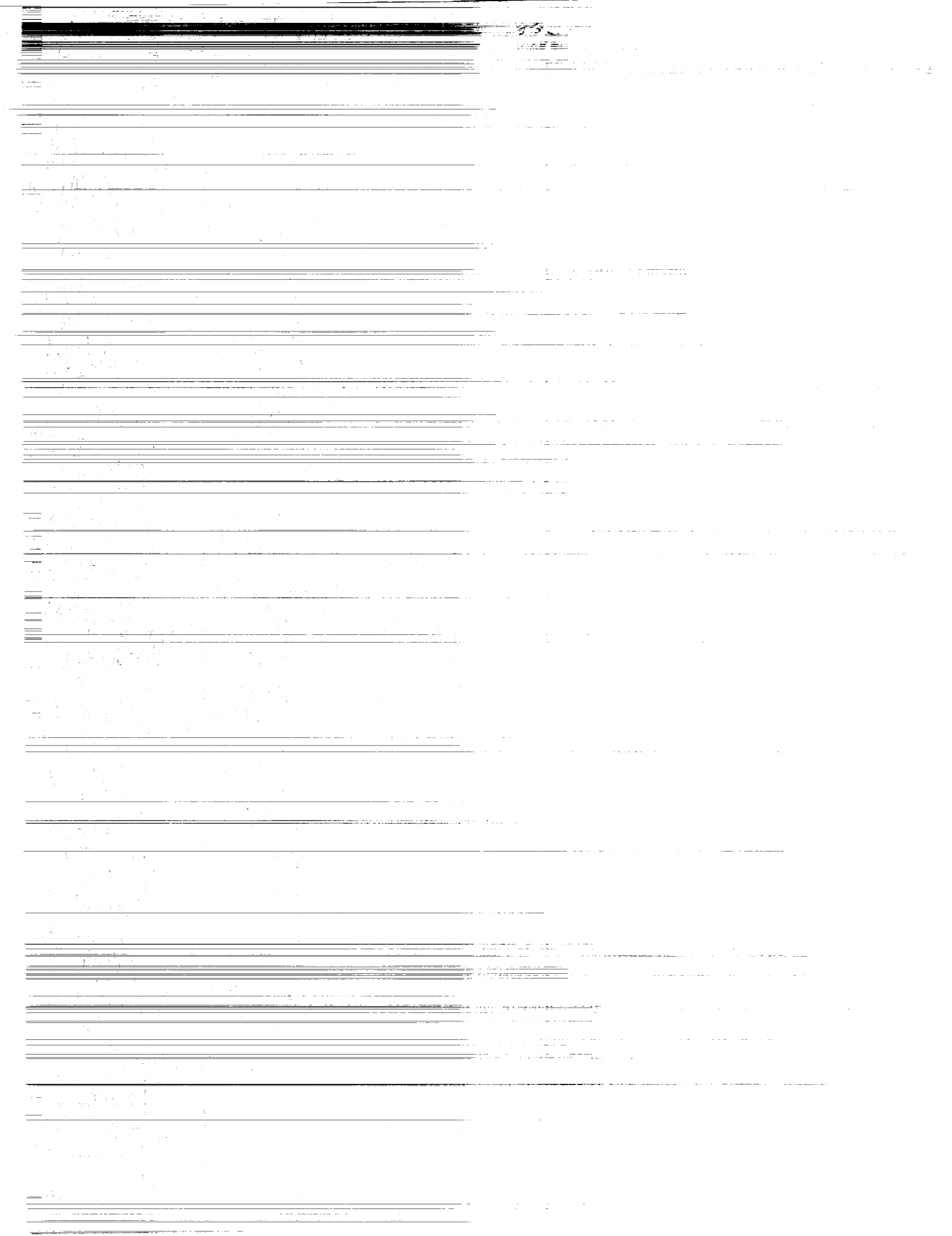

NASA Technical Paper 3146

1991

HZETRN: A Heavy Ion/Nucleon Transport Code for Space Radiations

John W. Wilson
Langley Research Center
Hampton, Virginia

Sang Y. Chun and Forooz F. Badavi
Old Dominion University
Norfolk, Virginia

Lawrence W. Townsend
Langley Research Center
Hampton, Virginia

Stanley L. Lamkin
Analytical Services & Materials, Inc.
Hampton, Virginia

NASA
National Aeronautics and Space Administration
Office of Management
Scientific and Technical Information Program

Abstract

The galactic heavy ion transport code (GCRTRN) *and the nucleon transport code* (BRYNTRN) *are integrated into a code package* (HZETRN). *The code package is computer efficient and capable of operating in an engineering design environment for manned deep space mission studies. The nuclear data set used by the code is discussed including current limitations. Although the heavy ion nuclear cross sections are assumed constant, the nucleon-nuclear cross sections of* BRYNTRN *with full energy dependence are used. The relation of the final code to the Boltzmann equation is discussed in the context of simplifying assumptions. Error generation and propagation is discussed, and comparison is made with simplified analytic solutions to test numerical accuracy of the final result. A brief discussion of biological issues and their impact on fundamental developments in shielding technology is given.*

1. Introduction

Propagation of galactic ions through matter has been studied for the past 40 years as a means of determining the origin of these ions. Peters (1958) used the one-dimensional equilibrium solution and ignored ionization energy loss and radioactive decay to show that the light ions have their origin in the breakup of heavy particles. Davis (1960) showed that one-dimensional propagation is simplistic and that leakage at the galactic boundary must be taken into account. Ginzburg and Syrovatskii (1964) argued that the leakage can be approximated as a superposition of nonequilibrium one-dimensional solutions. The "solution" to the steady-state equations is given as a Volterra equation by Gloeckler and Jokipii (1969), which is solved to first order in the fragmentation cross sections by ignoring energy loss. They provide an approximation to the first-order solution with ionization energy loss included that is only valid at relativistic energies. Lezniak (1979) gives an overview of cosmic ray propagation and derives a Volterra equation including the ionization energy loss which he refers to as a solution "only in the iterative sense" and evaluates only the unperturbed term. No attempt is made to evaluate either the first-order or higher order perturbation terms. The main interest among cosmic ray physicists has been in first-order solutions in the fragmentation cross sections, since path lengths in interstellar space are on the order of 3–4 g/cm^2. Clearly, higher order terms cannot be ignored in accelerator or space shielding transport problems (Wilson 1977a, 1977b, and 1983; Wilson et al. 1984). Aside from this simplification, the cosmic ray studies that were discussed have neglected the complicated three-dimensional nature of the fragmentation process.

Several approaches to the solution of high-energy heavy ion propagation including the ionization energy loss have been developed (Wilson 1977a, 1977b, and 1983; Wilson et al. 1984, 1989a, and 1987b; Wilson and Badavi 1986; Wilson and Townsend 1988; Curtis, Doherty, and Wilkinson 1969; Allkofer and Heinrich 1974; Chatterjee, Tobias, and Lyman 1976; Letaw, Tsao, and Silberberg 1983; Ganapol, Townsend, and Wilson 1989; Townsend, Ganapol, and Wilson 1989) over the last 20 years. All but one (Wilson 1977a) have assumed the straight ahead approximation and velocity conserving fragmentation interactions. Only two (Wilson 1977a; Wilson et al. 1984) have incorporated energy-dependent nuclear cross sections. The approach by Curtis, Doherty, and Wilkinson (1969) for a primary ion beam represented the first generation secondary fragments as a quadrature over the collision density of the primary beam. Allkofer and Heinrich (1974) used an energy multigroup method in which an energy-independent fragmentation transport approximation was applied within each energy group after which the energy group boundaries were moved according to continuous slowing down theory ($-dE/dx$). Chatterjee, Tobias, and Lyman (1976) solved the energy-independent fragment

transport equation with primary collision density as a source and neglected higher order fragmentation. The primary source term extended only to the primary ion range from the boundary. The energy-independent transport solution was modified to account for the finite range of the secondary fragment ions.

Wilson (1977b) derived an expression for the ion transport problem to first order (first collision term) and gave an analytic solution for the depth-dose relation. The more common approximations used in solving the heavy ion transport problem were further examined by Wilson (1977a). The effects of conservation of velocity on fragmentation and the straight ahead approximation are found to be negligible for cosmic ray applications. Solution methods for representing the energy-dependent nuclear cross sections are developed (Wilson 1977a). Letaw, Tsao, and Silberberg (1983) approximate the energy loss term and ion spectra by simple forms for which energy derivatives are evaluated explicitly (even if approximately). The resulting ordinary differential equations in position are solved analytically similar to the method of Allkofer and Heinrich (1974). This approximation results in a decoupling of motion in space and a change in energy. In Letaw's formalism, the energy shift is replaced by an effective attenuation factor. Wilson (1983) adds the next higher order (second collision) term. This term was found to be very important in describing ^{20}Ne beams at 670 MeV/amu. The three-term expansion was modified to include the effects of energy variation of the nuclear cross sections (Wilson et al. 1984). The integral form of the transport equation was also used to derive a numerical marching procedure to solve the cosmic ray transport problem (Wilson 1977a; Wilson and Badavi 1986). This method can easily include the energy-dependent nuclear cross sections within the numerical procedure. Comparison of the numerical procedure with an analytical solution to a simplified problem (Wilson and Badavi 1986; Wilson and Townsend 1988) validates the solution technique to about 1 percent accuracy. Several solution techniques and analytic methods have been developed for testing future numerical solutions to the transport equation (Ganapol, Townsend, and Wilson 1989; Townsend, Ganapol, and Wilson 1989). More recently, an analytic solution for the laboratory ion beam transport problem has been derived with a straight ahead approximation, velocity conservation at the interaction site, and energy-independent nuclear cross sections (Wilson et al. 1989a).

In this overview of past developments, the applications split into two separate categories according to a single ion species with a single energy at the boundary versus a broad host of elemental types with a broad, continuous energy spectrum. Techniques requiring a representation of the spectrum over an array of energy values require vast computer storage and computation speed for the laboratory beam problem to maintain sufficient energy resolution. On the other hand, analytic methods (Wilson 1977a) are probably best applied in a marching procedure (Wilson and Badavi 1986), which again has within it a similar energy resolution problem. This is a serious limitation because we require a final High Charge and Energy (HZE) Code for cosmic ray shielding that has been validated by laboratory experiments. There is some hope of having a single code which is able to be validated in the laboratory (Wilson et al. 1984; Schimmerling et al. 1989; Schimmerling 1990). More recently a Green's function has been derived which holds promise for a code which may be tested in the laboratory environment and applied to space radiation protection (Wilson et al. 1990).

In the present paper, we start with the general Boltzmann equation and simplify by using the standard assumptions to derive the straight ahead equation in the continuous slowing down approximation with the assumption that heavy projectile breakup conserves velocity. A numerical procedure is derived with the coupling of the heavy ions to the nucleon fields. Numerical stability and error propagation are discussed. Analytic benchmark solutions are used to test the numerical procedures. The nuclear data and nuclear models are presented. The general computational procedures and data base have been in use for GCR shielding studies

since about 1987. A discussion of related biological issues and their impact on the need for future code development is also given.

2. Boltzmann Equation

Since the volume of any material is mostly electrons, it is natural that most of the interactions of energetic ions passing through any material are with electrons. The cross section for the interactions of atomic electron σ^{at} is

$$\sigma^{at} \sim 10^{-16} \text{ cm}^2$$

The long range of the nuclear coulomb field also presents a sizable cross section σ^c to the passing ion

$$\sigma^c \sim 10^{-19} \text{ cm}^2$$

and ion collisions are dominated by these two processes but individual collisions have little effect on the passing ion.

Although most collisions in the material are coulomb collisions with orbital electrons and nuclei, the rare nuclear reactions are of importance because of the large energy transferred in the reaction and the generation of new energetic particles. This process of transferring kinetic energy into new secondary radiations occurs through several different processes, such as direct knockout of nuclear constituents, resonant excitation followed by particle emission, pair production, and possible coherent effects within the nucleus. Through these processes, a single particle incident on the shield may attenuate through energy transfer to electrons of the media or generate a multitude of secondaries causing an increase in exposure (transition effect). Which process dominates depends on energy, particle type, and material composition. This development of cascading particles is depicted in figure 2.1 as a relative comparison between high-energy proton and alpha particle cascades in the Earth's atmosphere. Note the similarities displayed in figure 2.1 for individual reaction events and the nuclear star events shown in figure 2.2 for nuclear emulsion (Krebs 1950).

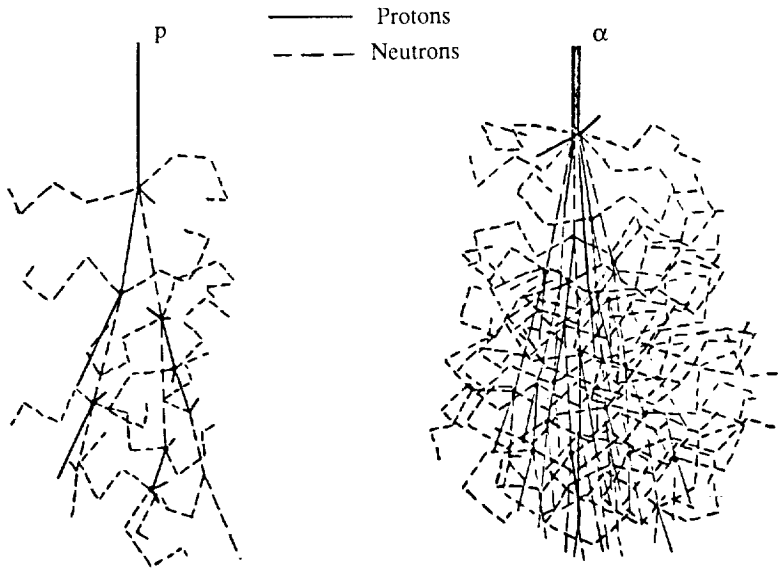

Figure 2.1. Cascade development in low Z materials.

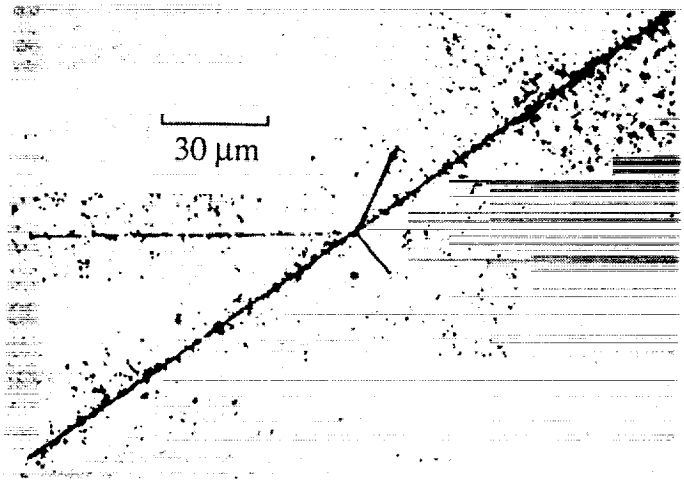

(a) $Z \approx 20$ projectile, low-energy transfer event.

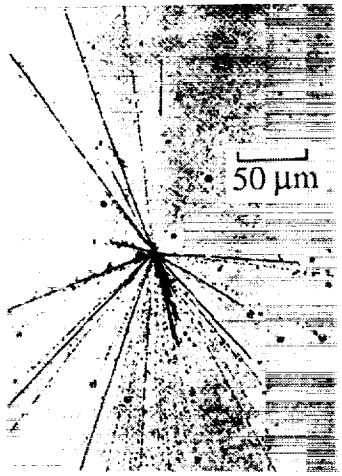

(b) Neutral primary, 27 relativistic charged prongs.

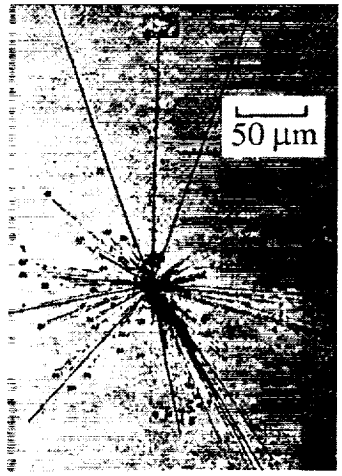

(c) $Z \approx 17$ projectile, high-energy transfer event.

Figure 2.2. Nuclear star events observed in nuclear emulsion (from Krebs 1950).

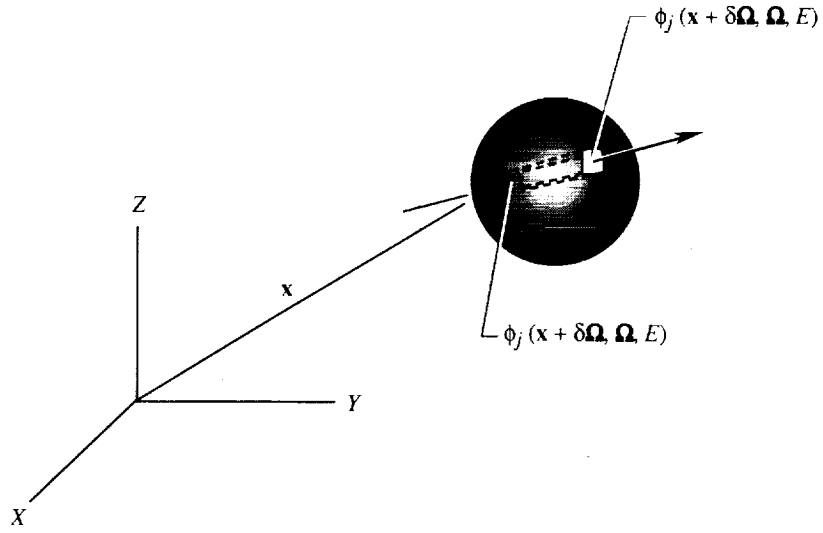

Figure 2.3. Transport of particles through spherical region.

The relevant transport equations are derived on the basis of conservation principles. Consider a region of space filled by matter described by appropriate atomic and nuclear cross sections. In figure 2.3, we show a small portion of the region enclosed by a sphere of radius δ. The number of particles of type j leaving a surface element $\delta^2\ d\mathbf{\Omega}$ is given as $\phi_j(\mathbf{x}+\delta\mathbf{\Omega},\mathbf{\Omega},E)\delta^2\ d\mathbf{\Omega}$ where $\phi_j(\mathbf{x},\mathbf{\Omega},E)$ is the particle flux density, $\mathbf{x}$ is a vector to the center of the sphere, $\mathbf{\Omega}$ is normal to the surface element, and E is the particle energy. The projection of the surface element through the sphere center to the opposite side of the sphere defines a flux tube through which pass a number of particles of type j given as $\phi_j(\mathbf{x}-\delta\mathbf{\Omega},\mathbf{\Omega},E)\delta^2\ d\mathbf{\Omega}$, which would equal the number leaving the opposite face if the tube defined by the projection were a vacuum. The two numbers of particles in fact differ by the gains and the losses created by atomic and nuclear collisions as follows:

$$\begin{aligned}\phi_j(\mathbf{x}+\delta\mathbf{\Omega},\mathbf{\Omega},E)\delta^2\ d\mathbf{\Omega} = \phi_j(\mathbf{x}-\delta\mathbf{\Omega},\mathbf{\Omega},E)\delta^2\ d\mathbf{\Omega}\\ + \delta^2\ d\mathbf{\Omega}\int_{-\delta}^{\delta} d\ell \sum_k \int \sigma_{jk}(\mathbf{\Omega},\mathbf{\Omega}',E,E')\ \phi_k(\mathbf{x}+\ell\mathbf{\Omega},\mathbf{\Omega}',E')\ d\mathbf{\Omega}'\ dE'\\ - \delta^2\ d\mathbf{\Omega}\int_{-\delta}^{\delta} d\ell\sigma_j(E)\ \phi_j(\mathbf{x}+\ell\mathbf{\Omega},\mathbf{\Omega},E) \qquad (2.1)\end{aligned}$$

where $\sigma_j(E)$ and $\sigma_{jk}(\mathbf{\Omega},\mathbf{\Omega}',E,E')$ are the media macroscopic cross sections. The cross section $\sigma_{jk}(\mathbf{\Omega},\mathbf{\Omega}',E,E')$ represents all those processes by which type k particles moving in direction $\mathbf{\Omega}'$ with energy E' produce a type j particle in direction $\mathbf{\Omega}$ with energy E. Note, there may be several reactions which may accomplish this result and the appropriate cross sections of equation (2.1) are the inclusive ones. Note that the second term on the right-hand side of equation (2.1) is the source of secondary particles integrated over the total volume $2\delta(\delta^2\ d\mathbf{\Omega})$ and the third term is the loss through nuclear reaction integrated over the same volume. We expand the terms of each side and retain terms to order δ^3 explicitly as

$$\begin{aligned}\delta^2\ d\mathbf{\Omega}\left[\phi_j(\mathbf{x},\mathbf{\Omega},E) + \delta\mathbf{\Omega}\cdot\nabla\phi_j(\mathbf{x},\mathbf{\Omega},E)\right] = \delta^2\ d\mathbf{\Omega}\left[\phi_j(\mathbf{x},\mathbf{\Omega},E) - \delta\mathbf{\Omega}\cdot\nabla\phi_j(\mathbf{x},\mathbf{\Omega},E)\right.\\ + 2\delta\sum_k \int \sigma_{jk}(\mathbf{\Omega},\mathbf{\Omega}',E,E')\ \phi_k(\mathbf{x},\mathbf{\Omega}',E')\ d\mathbf{\Omega}'\ dE'\\ \left.-2\delta\sigma_j(E)\ \phi_j(\mathbf{x},\mathbf{\Omega},E)\right] + O(\delta^4) \qquad (2.2)\end{aligned}$$

which may be divided by the cylindrical volume $2\delta(\delta^2\ d\mathbf{\Omega})$ and written as

$$\begin{aligned}\mathbf{\Omega}\cdot\nabla\phi_j(\mathbf{x},\mathbf{\Omega},E) = \sum_k \int \sigma_{jk}(\mathbf{\Omega},\mathbf{\Omega}',E,E')\phi_k(\mathbf{x},\mathbf{\Omega}',E')\ d\mathbf{\Omega}'\ dE'\\ - \sigma_j(E)\ \phi_j(\mathbf{x},\mathbf{\Omega},E) + O(\delta) \qquad (2.3)\end{aligned}$$

for which the last term $O(\delta)$ approaches zero in the limit as $\delta \to 0$. Equation (2.3) is recognized as a time-independent form of the Boltzmann equation for a tenuous gas. Atomic collisions (i.e., collisions with atomic electrons) preserve the identity of the particle, and two terms of the right-hand side of equation (2.3) contribute. The differential cross sections have the approximate form for atomic processes

$$\sigma_{jk}^{\mathrm{at}}(\mathbf{\Omega},\mathbf{\Omega}',E,E') = \sum_n \sigma_{jn}^{\mathrm{at}}(E')\ \delta(\mathbf{\Omega}\cdot\mathbf{\Omega}'-1)\ \delta_{jk}\ \delta(E+\epsilon_n-E') \qquad (2.4)$$

where n labels the electronic excitation levels and ϵ_n represents the corresponding excitation energies which are small (1–100 eV in most cases) compared with the particle energy E. The

atomic terms may then be written as

$$\begin{aligned}
&\sum_k \int \sigma_{jk}^{\mathrm{at}}(\mathbf{\Omega}, \mathbf{\Omega}', E, E')\ \phi_k(\mathbf{x}, \mathbf{\Omega}', E')\ d\mathbf{\Omega}'\ dE' - \sigma_j^{\mathrm{at}}(E)\ \phi_j(\mathbf{x}, \mathbf{\Omega}, E) \\
&\quad = \sum_n \sigma_{jn}^{\mathrm{at}}(E + \epsilon_n)\ \phi_j(\mathbf{x}, \mathbf{\Omega}, E + \epsilon_n) - \sigma_j^{\mathrm{at}}(E)\ \phi_j(\mathbf{x}, \mathbf{\Omega}, E) \\
&\quad \approx \sum_n \sigma_{jn}^{\mathrm{at}}(E)\ \phi_j(\mathbf{x}, \mathbf{\Omega}, E) + \sum_n \epsilon_n \frac{\partial}{\partial E}\left[\sigma_{jn}^{\mathrm{at}}(E)\ \phi_j(\mathbf{x}, \mathbf{\Omega}, E)\right] \\
&\qquad - \sigma_j^{\mathrm{at}}(E)\ \phi_j(\mathbf{x}, \mathbf{\Omega}, E) \\
&\quad = \frac{\partial}{\partial E}\left[S_j(E)\ \phi_j(\mathbf{x}, \mathbf{\Omega}, E)\right] \qquad (2.5)
\end{aligned}$$

since the stopping power is

$$S_j(E) = \sum_n \sigma_{jn}(E)\epsilon_n \qquad (2.6)$$

and the total atomic cross section is

$$\sigma_j^{\mathrm{at}}(E) = \sum_n \sigma_{jn}^{\mathrm{at}}(E) \qquad (2.7)$$

Equations (2.5) to (2.7) allow us to rewrite equation (2.3) in the usual continuous slowing down approximation as

$$\begin{aligned}
&\mathbf{\Omega} \cdot \nabla \phi_j(\mathbf{x}, \mathbf{\Omega}, E) - \frac{\partial}{\partial E}\left[S_j(E)\ \phi_j(\mathbf{x}, \mathbf{\Omega}, E)\right] + \sigma_j(E)\ \phi_j(\mathbf{x}, \mathbf{\Omega}, E) \\
&\quad = \int \sum_k \sigma_{jk}(\mathbf{\Omega}, \mathbf{\Omega}', E, E')\ \phi_k(\mathbf{x}, \mathbf{\Omega}', E')\ d\mathbf{\Omega}'\ dE' \qquad (2.8)
\end{aligned}$$

where the cross sections of equation (2.8) now contain only the nuclear contributions.

The purpose of the rest of this report concerns finding values for the atomic and nuclear cross sections, evaluating solutions to equation (2.8) for various boundary conditions, and making application to various radiation protection issues.

The response of materials to ionizing radiation is related to the amount of local energy deposited and the manner in which that energy is deposited. The energy given up to nuclear emulsion is shown for several ions in figure 2.4. The figure registers developable crystals caused by the passage of the particle directly by ionization or indirectly by the ionization of secondary electrons (δ-rays). These δ-rays appear as hairs emanating from the particle track. Note that the scale of the δ-ray track is on the order of biological cell dimensions (2–10 μm). Many of the modern large integrated circuits are even of the 0.5 μm scale. For this scale, track structure effects become important as interruptive events as a particle passes through active elements of such circuits.

From the radiation protection perspective, the issues of shielding are somewhat clearly drawn. Given the complex external environment, the shield properties alter the internal environment within the spacecraft structure as shown in figure 2.5. The internal environment within the spacecraft interacts with onboard personnel or equipment. If sufficient knowledge is known about specific devices and biological response, then the shield properties can be altered so as to minimize adverse affects. Since the shield is intimately connected to the overall engineering systems and often impacts launch cost, the minimization of radiation risk is not independent of other risk factors and mission cost. Even mission objectives are at times impacted by radiation

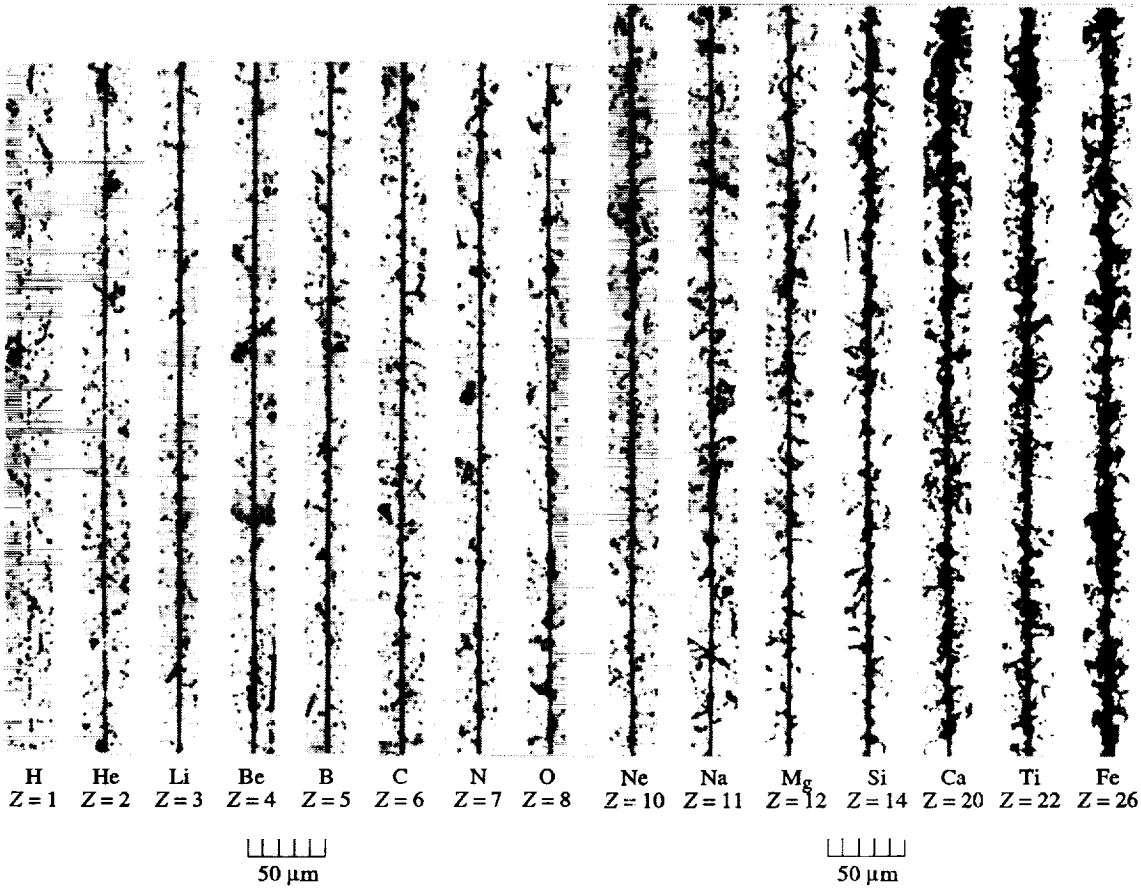

Figure 2.4. Ionization tracks of energetic cosmic ions.

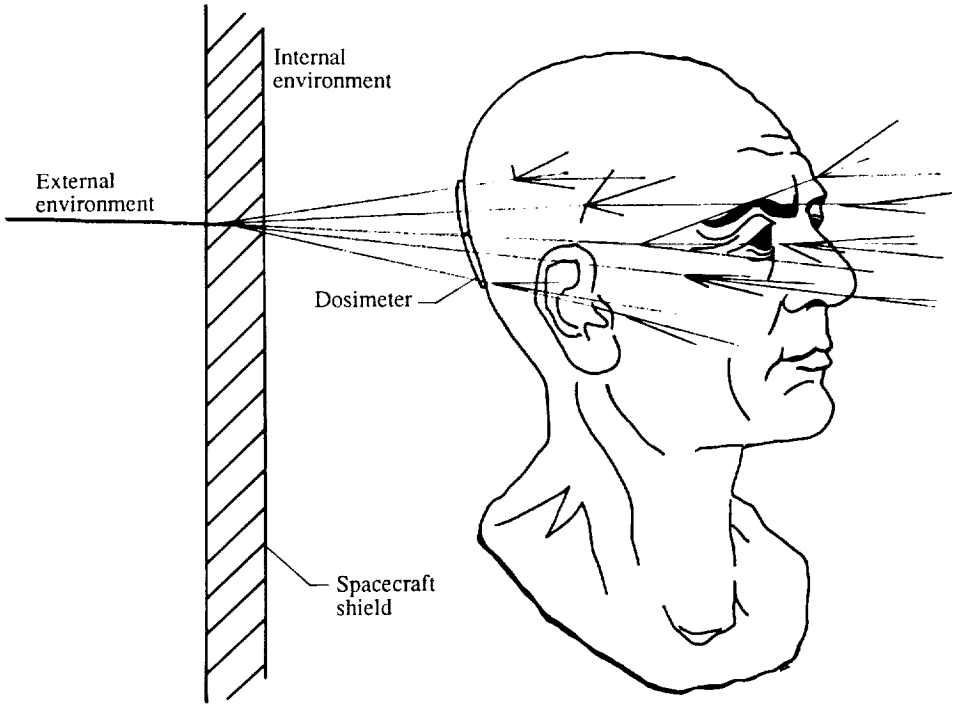

Figure 2.5. Schematic of the cosmic ray protection problem.

protection requirements (e.g., the Viking solar cell design to ensure sufficient solar power in the event of decreased performance caused by a large solar flare during the mission affected the weight allowed the experiments package). The uncertainty in shield specification is clearly an important factor when such critical issues are being addressed. There is uncertainty in subsystem response which can be easily (more or less) obtained for electronic or structural devices. The uncertainty in response of biological systems is complicated by the long delay times (up to 30 years) before system response occurs and the unusually small signal-to-noise ratio in biological response. Clearly a difficult task remains before risk assignments can be made for long duration deep space missions.

3. Transport Formalism

The Boltzmann equation in the continuous slowing approximation is given by

$$\left[\mathbf{\Omega}\cdot\nabla - \frac{1}{A_j}\frac{\partial}{\partial E}S_j(E) + \sigma_j(E)\right]\,\phi_j\left(\mathbf{x},\mathbf{\Omega},E\right) = \sum_k \int dE'\; d\mathbf{\Omega}'\;\sigma_{jk}\left(E,E',\mathbf{\Omega},\mathbf{\Omega}'\right)\;\phi_k\left(\mathbf{x},\mathbf{\Omega}',E'\right) \tag{3.1}$$

where $\phi_j\left(\mathbf{x},\mathbf{\Omega},E\right)$ is the flux of ions of type j with atomic mass A_j at $\mathbf{x}$ with motion along $\mathbf{\Omega}$ and energy E in units of MeV/amu (note that the energy units of eq. (2.8) are MeV), $\sigma_j(E)$ is the corresponding macroscopic cross section, $S_j(E)$ is the linear energy transfer (LET), and $\sigma_{jk}\left(E,E',\mathbf{\Omega},\mathbf{\Omega}'\right)$ is the production cross section for type j particles with energy E and direction $\mathbf{\Omega}$ by the collision of type k particle of energy E' and direction $\mathbf{\Omega}'$. The term on the left-hand side of equation (3.1) containing $S_j(E)$ is a result of the continuous slowing down approximation, whereas the remaining terms of equation (3.1) are the usual Boltzmann terms. The solutions to equation (3.1) are unique in any convex region for which the inbound flux of each particle type is specified everywhere on the bounding surface. If the boundary is given as the loci of the two-parameter vector function $\gamma(s,t)$ for which a generic point on the boundary is given by $\mathbf{\Gamma}$, then the boundary condition is specified by requiring the solution of equation (3.1) to meet

$$\phi_j(\mathbf{\Gamma},\mathbf{\Omega},E) = \psi_j(\mathbf{\Gamma},\mathbf{\Omega},E) \tag{3.2}$$

for each value of $\mathbf{\Omega}$ such that

$$\mathbf{\Omega}\cdot\mathbf{n}(\mathbf{\Gamma}) < 0 \tag{3.3}$$

where $\mathbf{n}(\mathbf{\Gamma})$ is the outward-directed unit normal vector to the boundary surface at the point $\mathbf{\Gamma}$ and ψ_j is a specified boundary function.

The fragmentation of the projectile and target nuclei is represented by the quantities $\sigma_{jk}\left(E,E',\mathbf{\Omega},\mathbf{\Omega}'\right)$, which are composed of three functions:

$$\sigma_{jk}\left(E,E',\mathbf{\Omega},\mathbf{\Omega}'\right) = \sigma_k(E')\;\nu_{jk}(E')\;f_{jk}\left(E,E',\mathbf{\Omega},\mathbf{\Omega}'\right) \tag{3.4}$$

where $\nu_{jk}(E')$ is the average number (which we loosely refer to as multiplicity) of type j particles being produced by a collision of type k of energy E' and $f_{jk}\left(E,E',\mathbf{\Omega},\mathbf{\Omega}'\right)$ is the probability density distribution for producing particles of type j of energy E into direction $\mathbf{\Omega}$ from the collision of a type k particle with energy E' moving in direction $\mathbf{\Omega}'$. For an unpolarized source of projectiles and unpolarized targets, the energy angle distribution of reaction products may be a function of the energies and cosine of the production angle relative to the incident projectile direction. The secondary multiplicities $\nu_{jk}(E)$ and secondary energy angle distributions are the major unknowns in ion transport theory.

Information on the multiplicity $\nu_{jk}(E)$ was obtained in the past through experiments with galactic cosmic rays as an ion source, and the fragmentation of the ions on target nuclei was observed in nuclear emulsion (Cleghorn, Freier, and Waddington 1968). Such data are mainly limited by not knowing the identity of the initial or secondary ions precisely and by relatively low counting rates of each ion type. The heavy ion acceleration by machine makes a reduction in the uncertainty possible because large count rates can be obtained with known ion types. In addition, the accelerator experiments are providing information on the spectral distribution $f_{jk}\left(E, E', \mathbf{\Omega}, \mathbf{\Omega}'\right)$ which has not before been available (Heckman et al. 1972).

The spectral distribution function is found to consist of two terms that describe the fragmentation of the projectile and the fragmentation of the struck nucleus as follows (Heckman 1975; Raisbeck and Yiou 1975):

$$\sigma_{jk}\left(E, E', \mathbf{\Omega}, \mathbf{\Omega}'\right) = \sigma_k(E')\left[\nu_{jk}^P(E')\ f_{jk}^P\left(E, E', \mathbf{\Omega}, \mathbf{\Omega}'\right) + \nu_{jk}^T(E')\ f_{jk}^T\left(E, E', \mathbf{\Omega}, \mathbf{\Omega}'\right)\right] \tag{3.5}$$

where ν_{jk}^P and f_{jk}^P depend only weakly on the target and ν_{jk}^T and f_{jk}^T depend only weakly on the projectile. Although the average secondary velocities associated with f^P are nearly equal to the projectile velocity, the average velocities associated with f^T are near zero. Experimentally, Heckman (1975) observed that

$$\begin{aligned} f_{jk}^P\left(E, E', \mathbf{\Omega}, \mathbf{\Omega}'\right) &\approx \left[\frac{m}{2\pi\left(\sigma_{jk}^P\right)^2}\right]^{3/2} \sqrt{2E}\exp\left[-\frac{(\mathbf{p}-\mathbf{p}')^2}{2\left(\sigma_{jk}^P\right)^2}\right] \\ &\approx \left[\frac{m}{2\pi\left(\sigma_{jk}^P\right)^2}\right]^{3/2} \sqrt{2E}\exp\left[-\frac{\left(\mathbf{\Omega}\sqrt{2mE} - \mathbf{\Omega}'\sqrt{2mE'}\right)^2}{2\left(\sigma_{jk}^P\right)^2}\right] \end{aligned} \tag{3.6}$$

where $\mathbf{p}$ and $\mathbf{p}\prime$ are the momenta per unit mass of j and k ions, respectively, and

$$f_{jk}^T\left(E, E', \mathbf{\Omega}, \mathbf{\Omega}'\right) \approx \left[\frac{m}{2\pi\left(\sigma_{jk}^T\right)^2}\right]^{3/2} \sqrt{2E}\exp\left[-\frac{\mathbf{p}^2}{2\left(\sigma_{jk}^T\right)^2}\right] \tag{3.7}$$

where σ_{jk}^P and σ_{jk}^T are related to the root mean square (rms) momentum spread of secondary products. These parameters depend only on the fragmenting nucleus. Feshbach and Huang (1973) suggested that the parameters σ_{jk}^P and σ_{jk}^T depend on the average square momentum of the nuclear fragments as allowed by Fermi motion. A precise formulation of these ideas in terms of a statistical model was obtained by Goldhaber (1974).

4. Approximation Procedures

4.1. Neglect of Target Fragmentation

Using equations (3.5), (3.6), and (3.7) in the evaluation of the source term $\zeta_j\left(\mathbf{x}, \mathbf{\Omega}, E\right)$ of equation (3.1) results in

$$\begin{aligned} \zeta_j\left(\mathbf{x}, \mathbf{\Omega}, E\right) &= \sum_k \int dE'\ d\mathbf{\Omega}'\ \sigma_k(E')\ \phi_k\left(\mathbf{x}, \mathbf{\Omega}', \mathbf{E}'\right)\left[\nu_{jk}^P(E')\ f_{jk}^P\left(E, E', \mathbf{\Omega}, \mathbf{\Omega}'\right)\right. \\ &\quad \left. + \nu_{jk}^T\ f_{jk}^T\left(E, E', \mathbf{\Omega}, \mathbf{\Omega}'\right)\right] \\ &\equiv \zeta_j^P\left(\mathbf{x}, \mathbf{\Omega}, E\right) + \zeta_j^T\left(\mathbf{x}, \mathbf{\Omega}, E\right) \end{aligned} \tag{4.1}$$

where, as before, the superscripts P and T refer to fragmentation of the projectile and target, respectively. The target term is

$$\zeta_j^T(\mathbf{x},\mathbf{\Omega},E) = \sum_k \left[\frac{m}{2\pi\left(\sigma_{jk}^T\right)^2}\right]^{3/2} \sqrt{2E}\exp\left[\frac{-mE}{\left(\sigma_{jk}^T\right)^2}\right]$$
$$\times \int d\mathbf{\Omega}' \int_E^\infty dE'\ \nu_{jk}^T(E')\ \sigma_k(E')\ \phi_k(\mathbf{x},\mathbf{\Omega}',E') \tag{4.2}$$

which is negligibly small for

$$E \gg \frac{\left(\sigma_{jk}^T\right)^2}{m} \tag{4.3}$$

Thus, for calculating the flux at high energy,

$$\zeta_j(\mathbf{x},\mathbf{\Omega},E) \approx \zeta_j^P(\mathbf{x},\mathbf{\Omega},E) \tag{4.4}$$

4.2. Space Radiations

A convenient property of space radiations is that they are nearly isotropic. This fact, coupled with the forward peaked spectral distribution, leads to substantial reductions in the source term as follows:

$$\zeta_j^P(\mathbf{x},\mathbf{\Omega},E) \approx \sum_k \int dE'\ d\mathbf{\Omega}'\ \sigma_k(E')\ \nu_{jk}^P(E') \left[\frac{m}{2\pi\left(\sigma_{jk}^P\right)^2}\right]^{3/2} \sqrt{2E'}$$
$$\times \exp\left[-\frac{\left(\mathbf{\Omega}\sqrt{2mE} - \mathbf{\Omega}\sqrt{2mE'}\right)^2}{2\left(\sigma_{jk}^P\right)^2}\right] \phi_k(\mathbf{x},\mathbf{\Omega}',E') \tag{4.5}$$

If $\phi_k(\mathbf{x},\mathbf{\Omega}',E')$ is assumed to be a slowly varying function of $\mathbf{\Omega}'$, one may seek an expansion about the sharply peaked maximum of the exponential function. Such an expansion is made by letting

$$\mathbf{\Omega}' = \mathbf{\Omega} + (\cos\theta - 1)\mathbf{\Omega} + \mathbf{e}_\phi \sin\theta \tag{4.6}$$

where

$$\cos\theta = \mathbf{\Omega}\cdot\mathbf{\Omega}' \tag{4.7}$$

and

$$\mathbf{e}_\phi = \frac{\mathbf{\Omega}\times\mathbf{\Omega}'}{|\mathbf{\Omega}\times\mathbf{\Omega}'|} \tag{4.8}$$

The flux may be expanded as

$$\phi_k(\mathbf{x},\mathbf{\Omega}',E') = \phi_k(\mathbf{x},\mathbf{\Omega},E') + \left[\frac{\partial}{\partial\mathbf{\Omega}}\ \phi_k(\mathbf{x},\mathbf{\Omega},E')\right]\cdot\left[(\cos\theta - 1)\mathbf{\Omega} + \mathbf{e}_\phi\sin\theta\right] + \ldots \tag{4.9}$$

Substituting equation (4.9) into equation (4.5) and simplifying result in

$$\zeta_j^P(\mathbf{x},\mathbf{\Omega},E) \approx \sum_k \int dE'\ \sigma_k(E')\ \nu_{jk}^P(E') \left[\frac{m}{2\pi\left(\sigma_{jk}^P\right)^2}\right]^{3/2} \frac{\sqrt{2}}{\sqrt{E'}} \exp\left[-\frac{\left(\sqrt{2mE}-\sqrt{2mE'}\right)^2}{2\left(\sigma_{jk}^P\right)^2}\right]$$

$$\times \left\{\phi_k(\mathbf{x},\mathbf{\Omega},E') - \left[\mathbf{\Omega}\cdot\frac{\partial}{\partial\mathbf{\Omega}}\ \phi_k(\mathbf{x},\mathbf{\Omega},E')\right]\left[\frac{\left(\sigma_{jk}^P\right)^2}{2m\sqrt{EE'}}\right] + \ldots\right\} \tag{4.10}$$

The leading term of equation (4.10) is clearly a good approximation to the source term whenever

$$\frac{2mE}{\left(\sigma_{jk}^P\right)^2} \gg \frac{\mathbf{\Omega}\cdot\frac{\partial}{\partial\mathbf{\Omega}}\ \phi_k(\mathbf{x},\mathbf{\Omega},E')}{\phi_k(\mathbf{x},\mathbf{\Omega},E')} \tag{4.11}$$

The leading term is equivalent to assuming that secondary ions are produced only in the direction of motion of the primary ions. For space radiations which are nearly isotropic, relation (4.11) is easily met, and neglect of higher order terms in equation (4.10) results in the usual straight ahead approximation. If the radiation is highly anisotropic, then relation (4.11) is not likely to apply. Validity of the straight ahead approximation was discovered empirically by Alsmiller et al. (1965) and Alsmiller, Irving, and Moran (1968) for proton transport.

4.3. Velocity Conserving Interaction

Customarily, in cosmic ion transport studies (Curtis and Wilkinson 1972), the fragment velocities are assumed to be equal to the fragmenting ion velocity before collision. The order of approximation resulting from such an assumption is derived. Since the projectile energy E' is assumed to be equal to the secondary energy plus a positive quantity ϵ,

$$E' = E + \epsilon \tag{4.12}$$

and ϵ is assumed to contribute to equation (4.10) only over a small range above zero energy, substituting equation (4.12) into equation (4.10) and expanding the integrand result in

$$\zeta_j^P(\mathbf{x},\mathbf{\Omega},E) = \sum_k \sigma_k(E)\ \nu_{jk}^P(E) \left\{\phi_k(\mathbf{x},\mathbf{\Omega},E)\left[1-\sqrt{\frac{\left(\sigma_{jk}^P\right)^2}{\pi mE}}\right]\right.$$

$$\left. + \left[E\frac{\partial}{\partial E}\ \phi_k(\mathbf{x},\mathbf{\Omega},E)\right]\sqrt{\frac{\left(\sigma_{jk}^P\right)^2}{\pi mE}} - \left[\mathbf{\Omega}\cdot\frac{\partial}{\partial\mathbf{\Omega}}\ \phi_k(\mathbf{x},\mathbf{\Omega},E)\right]\frac{\left(\sigma_{jk}^P\right)^2}{2mE} + \ldots\right\} \tag{4.13}$$

Because $\sqrt{\left(\sigma_{jk}^P\right)^2/mE} \ll 1$ at those energies for which most nuclear reactions occur, the assumption of velocity conservation is clearly inferior to a straight ahead approximation but may be adequate for space radiations where the variation of $\phi_k(\mathbf{x},\mathbf{\Omega},E)$ with energy is sufficiently smooth. That is,

$$E\ \frac{\partial}{\partial E}\ \phi_k(\mathbf{x},\mathbf{\Omega},E) \approx \phi_k(\mathbf{x},\mathbf{\Omega},E)$$

4.4. Decoupling of Target and Projectile Flux

Equation (3.1) with the use of equation (4.1) may be rewritten as

$$B_j \phi_j (\mathbf{x}, \mathbf{\Omega}, E) = \sum_k F_{jk}^T \ \phi_k (\mathbf{x}, \mathbf{\Omega}, E) + \sum_k F_{jk}^P \ \phi_k (\mathbf{x}, \mathbf{\Omega}, E) \tag{4.14}$$

where the differential operator is given by

$$B_j = \left[\mathbf{\Omega} \cdot \nabla - \frac{1}{A_j} \frac{\partial}{\partial E} S_j(E) + \sigma_j(E) \right] \tag{4.15}$$

and the integral operator $\left(F_{jk} = F_{jk}^T + F_{jk}^P \right)$ is given by

$$F_{jk} \ \phi_k (\mathbf{x}, \mathbf{\Omega}, E) = \int dE' \ d\mathbf{\Omega}' \ \sigma_{jk} (E, E', \mathbf{\Omega}, \mathbf{\Omega}') \ \phi_k (\mathbf{x}, \mathbf{\Omega}', E') \tag{4.16}$$

Defining the flux as a sum of two terms

$$\phi_j (\mathbf{x}, \mathbf{\Omega}, E) = \phi_j^T (\mathbf{x}, \mathbf{\Omega}, E) + \phi_j^P (\mathbf{x}, \mathbf{\Omega}, E) \tag{4.17}$$

allows the following separation:

$$B_j \ \phi_j^P (\mathbf{x}, \mathbf{\Omega}, E) = \sum_k F_{jk}^P \ \phi_k^P (\mathbf{x}, \mathbf{\Omega}, E) + \sum_k F_{jk}^P \ \phi_k^T (\mathbf{x}, \mathbf{\Omega}, E) \tag{4.18}$$

$$B_j \ \phi_j^T (\mathbf{x}, \mathbf{\Omega}, E) = \sum_k F_{jk}^T \ \phi_k^P (\mathbf{x}, \mathbf{\Omega}, E) + \sum_k F_{jk}^T \ \phi_k^T (\mathbf{x}, \mathbf{\Omega}, E) \tag{4.19}$$

As noted in connection with equations (4.1) through (4.4), the source term on the right-hand side of equation (4.19) is small at high energies and one may assume

$$\phi_j^T (\mathbf{x}, \mathbf{\Omega}, E) \approx 0 \tag{4.20}$$

for $E \gg (\sigma_{jk}^T)^2/m$. As a result of equation (4.20) and the fact that the ion range is small compared with its mean free path at low energy, one obtains

$$B_j \ \phi_j^P (\mathbf{x}, \mathbf{\Omega}, E) \approx \sum_k F_{jk}^P \ \phi_k^P (\mathbf{x}, \mathbf{\Omega}, E) \tag{4.21}$$

$$B_j \ \phi_j^T (\mathbf{x}, \mathbf{\Omega}, E) \approx \sum_k F_{jk}^T \ \phi_k^P (\mathbf{x}, \mathbf{\Omega}, E) \tag{4.22}$$

The advantage of this separation is that once equation (4.21) is solved by whatever means necessary, then equation (4.22) can be solved in closed form. The solution of equation (4.22) is accomplished by noting that the inwardly directed flux ϕ_j^T must vanish on the boundary so that

$$\begin{aligned} \phi_j^T (\mathbf{x}, \mathbf{\Omega}, E) \approx \sum_k \int_E^{E_\gamma} dE' \ \frac{A_j P_j(E')}{P_j(E) S_j(E)} \int dE'' \ d\mathbf{\Omega} \ \sigma_{jk}^T (E', E'', \mathbf{\Omega}, \mathbf{\Omega}') \\ \times \phi_k^P \left\{ \mathbf{x} + \left[R_j(E) - R_j(E') \right] \mathbf{\Omega}, \mathbf{\Omega}', E'' \right\} \end{aligned} \tag{4.23}$$

where $E_\gamma = R_j^{-1}[d + R_j(E)]$ with d the projected distance to the boundary.

Using equations (3.5) and (3.7) in equation (4.23) yields

$$\phi_j^T(\mathbf{x},\mathbf{\Omega},E) \approx \int_E^{E_\gamma} dE' \frac{A_j\ P_j(E')}{P_j(E)\ S_j(E)} \left[\frac{m}{2\pi\left(\sigma_{jk}^T\right)^2}\right]^{3/2} \sqrt{2E'} \exp\left[\frac{-mE'}{\left(\sigma_{jk}^T\right)^2}\right] \times \zeta_j^T\left\{\mathbf{x} + \left[R_j(E) - R_j(E')\right]\mathbf{\Omega}\right\} \tag{4.24}$$

where

$$\zeta_j^T(\mathbf{x}) = \sum_k \int dE'\ d\mathbf{\Omega}'\ \sigma_k(E')\ \nu_{jk}^T(E')\ \phi_k^P(\mathbf{x},\mathbf{\Omega}',E') \tag{4.25}$$

and σ_{jk}^T has been assumed to be a slowly varying function of projectile type k and projectile energy E. If the range of secondary type j ions is small compared with their mean free path lengths and the mean free paths of the fragmenting parent ions ℓ_k, that is,

$$R_j\left[\frac{\left(\sigma_{jk}^T\right)^2}{m}\right] \ll \ell_k \tag{4.26}$$

then the integral of equation (4.24) may be simplified as

$$\phi_j^T(\mathbf{x},\mathbf{\Omega},E) \approx \frac{A_j}{S_j(E)}\ \zeta_j^T(\mathbf{x}) \int_E^{E_\gamma} \left[\frac{m}{2\pi\left(\sigma_{jk}^T\right)^2}\right]^{3/2} \sqrt{2E'} \exp\left[\frac{-mE'}{\left(\sigma_{jk}^T\right)^2}\right] dE' \tag{4.27}$$

which may be reduced into terms of known functions. Thus,

$$\phi_j^T(\mathbf{x},\mathbf{\Omega},E) \approx \frac{A_j}{S_j(E)}\ \zeta_j^T(\mathbf{x})\ \frac{1}{2\pi\sqrt{\pi}} \left\{\Gamma\left[\frac{3}{2}, \frac{mE}{\left(\sigma_{jk}^T\right)^2}\right] - \Gamma\left[\frac{3}{2}, \frac{mE_\gamma}{\left(\sigma_{jk}^T\right)^2}\right]\right\} \tag{4.28}$$

in terms of the incomplete gamma function. One can show that equation (3.28) is equivalent to

$$\phi_j^T(\mathbf{x},\mathbf{\Omega},E) \approx \frac{A_j}{S_j(E)}\ \zeta_j^T(\mathbf{x})\ \frac{1}{2\pi} \left\{\frac{1}{2}\ \mathrm{erfc}\left[\sqrt{\frac{mE}{\left(\sigma_{jk}^T\right)^2}}\right] - \frac{1}{2}\ \mathrm{erfc}\left[\sqrt{\frac{mE_\gamma}{\left(\sigma_{jk}^T\right)^2}}\right] + \sqrt{\frac{mE}{\pi\left(\sigma_{jk}^T\right)^2}} \exp\left[\frac{-mE}{\left(\sigma_{jk}^T\right)^2}\right] - \sqrt{\frac{mE_\gamma}{\pi\left(\sigma_{jk}^T\right)^2}} \exp\left[\frac{-mE\sigma}{\left(\sigma_{jk}^T\right)^2}\right]\right\} \tag{4.29}$$

At points sufficiently removed from the boundary such that

$$R_j^{-1}(d) \gg \frac{\left(\sigma_{jk}^T\right)^2}{m} \tag{4.30}$$

equation (4.28) may be reduced to

$$\phi_j^T(\mathbf{x},\mathbf{\Omega},E) \approx \frac{A_j}{S_j(E)}\,\zeta_j^T(\mathbf{x})\frac{1}{2\pi}\left\{\frac{1}{2}\,\mathrm{erfc}\left[\sqrt{\frac{mE}{\left(\sigma_{jk}^T\right)^2}}\right]+\sqrt{\frac{mE}{\pi\left(\sigma_{jk}^T\right)^2}}\,\exp\left[\frac{-mE}{\left(\sigma_{jk}^T\right)^2}\right]\right\} \tag{4.31}$$

The solution of equation (4.21) is now examined further.

4.5. Back-Substitution and Perturbation Theory

One approach to the solution of equation (4.21) results from the fact that the multiple-charged ions tend to be destroyed in nuclear reactions. Thus,

$$F_{jk}^P \equiv 0 \qquad\qquad (j \geq k) \tag{4.32}$$

This means that there is a maximum j such that

$$B_J\;\phi_J^P(\mathbf{x},\mathbf{\Omega},E) = 0 \tag{4.33}$$

where J is the largest j. Furthermore,

$$B_{J-1}\;\phi_{J-1}^P(\mathbf{x},\mathbf{\Omega},E) = F_{J-1,J}^P\;\phi_J^P(\mathbf{x},\mathbf{\Omega},E) \tag{4.34}$$

and, in general,

$$B_{J-N}\;\phi_{J-N}^P(\mathbf{x},\mathbf{\Omega},E) = \sum_{k=1}^{N-1} F_{J-N,J-k}^P\;\phi_{J-k}^P(\mathbf{x},\mathbf{\Omega},E) \tag{4.35}$$

for $N < J-1$. Note that equations (4.34) and (4.35) constitute solvable problems. The singly charged ions satisfy

$$B_1\;\phi_1^P(\mathbf{x},\mathbf{\Omega},E) = F_{1,1}^P\;\phi_1^P(\mathbf{x},\mathbf{\Omega},E) + \sum_{k=2}^{J} F_{1,k}^P\;\phi_k^P(\mathbf{x},\mathbf{\Omega},E) \tag{4.36}$$

which, unlike equations (4.33) to (4.35), is an integral-differential equation that is difficult to solve directly. Equation (4.35) is solvable by perturbation theory, and the resultant series is known to converge rapidly for intermediate and low energies (Wilson and Lamkin 1975; Wilson et al. 1989a and 1989b; Wilson and Townsend 1988). Note that equations (4.33) and (4.35) are also obtained from perturbation theory as applied to equation (4.21) at the outset. Thus, the perturbation series is expected to converge after the first J plus a few terms.

5. Galactic Ion Transport

In the present section, we expand on the methods developed earlier for nucleon transport (Wilson and Lamkin 1975) by combining analytic and numerical tools. The galactic cosmic ray ion transport problem is transformed to an integral along the characteristic curve of that particular ion. As a result of the conservation of velocity in fragmentation, the perturbation series (Wilson and Lamkin 1975) is replaced by a simple numerical procedure. The resulting method reduces the difficulty associated with the low-energy discretization and the restriction to a definite form for the stopping power. The resulting numerical computation is simple and nondemanding from computer requirements and yet gives superior results compared with other methods.

In the present work, we use the straight ahead approximation and neglect the target secondary fragments (Wilson 1977a and 1983). For multiply charged ions, the transport equation may be written as

$$\left[\frac{\partial}{\partial x} - \frac{\partial}{\partial E}\,\widetilde{S}_j(E) + \sigma_j\right]\phi_j(x,E) = \sum_{k>j} m_{jk}\sigma_k\;\phi_k(x,E) \tag{5.1}$$

where $\phi_j(x,E)$ is the flux of ions of type j with atomic mass A_j at x moving along the x axis at energy E in units of MeV/amu, σ_j is the corresponding macroscopic nuclear absorption cross section, $\widetilde{S}_j(E)$ is the change in E per unit distance, and m_{jk} is the multiplicity of ion j produced in collision by ion k. The corresponding nucleon transport equation is

$$\left[\frac{\partial}{\partial x} - \frac{\partial}{\partial E}\,\widetilde{S}_j(E) + \sigma_j(E)\right]\phi_j(x,E) = \sum_{k} \int_E^\infty \sigma_{jk}(E,E')\;\phi_k(x,E')\;dE' \tag{5.2}$$

The quantities m_{jk} and σ_j are assumed energy independent in equation (5.1) but are fully energy dependent in equation (5.2).

The range of the ion is given as

$$R_j(E) = \int_0^E \frac{dE'}{\widetilde{S}_j(E')} \tag{5.3}$$

The solution to equation (5.2) is found to be subject to boundary specification at $x = 0$ and arbitrary E as

$$\phi_j(0,E) = F_j(E) \tag{5.4}$$

Usually, $F_j(E)$ is called the incident beam spectrum.

From Bethe's theory,

$$\widetilde{S}_j(E) = \frac{A_p Z_j^2}{A_j Z_p^2}\;\widetilde{S}_p(E) \tag{5.5}$$

and holds for all energies above 100 keV/amu provided the ions remain fully stripped. It follows that

$$\frac{Z_j^2}{A_j}\;R_j(E) = \frac{Z_p^2}{A_p}\;R_p(E) \tag{5.6}$$

The subscript p refers to proton. Equation (5.6) is quite accurate at high energy and only approximately true at low energy because of electron capture by the ion which effectively reduces its charge, higher order Born corrections to Bethe's theory, and nuclear stopping at the lowest energies. Herein, the parameter ν_j is defined as

$$\nu_j\;R_j(E) = \nu_k\;R_k(E) \tag{5.7}$$

so that

$$\nu_j = \frac{Z_j^2}{A_j} \tag{5.8}$$

Equations (5.6) to (5.8) are used in the subsequent development, and the energy variation in ν_j is neglected. The inverse function of $R_j(E)$ is defined as

$$E = R_j^{-1}\left[R_j(E)\right] \tag{5.9}$$

A method of solution is now discussed. For the purpose of solving equation (5.2), define the coordinates

$$\eta_j \equiv x - R_j(E) \tag{5.10}$$

$$\xi_j \equiv x + R_j(E) \tag{5.11}$$

where η_j varies along the particle path and ξ_j is constant along the particle trajectory. The new fluence functions are taken as

$$\chi_j(\eta_j, \xi_j) \equiv \widetilde{S}_j(E)\ \phi_j(x, E) = \psi_j(x, r_j) \tag{5.12}$$

$$\overline{\chi}_k(\eta_j, \xi_j) \equiv \chi_k(\eta_k, \xi_k) \tag{5.13}$$

where

$$\xi_j + \eta_j = \xi_k + \eta_k \tag{5.14}$$

$$\eta_j - \xi_j = \frac{\nu_k}{\nu_j}(\eta_k - \xi_k) \tag{5.15}$$

and $r_j = R_j(E)$. Under this coordinate mapping, equation (5.1) becomes

$$\left[2\frac{\partial}{\partial \eta_j} + \sigma_j\right]\ \chi_j(\eta_j, \xi_j) = \sum_k m_{jk}\sigma_k \frac{\nu_j}{\nu_k}\ \overline{\chi}_k(\eta_j, \xi_j) \tag{5.16}$$

where σ_j is assumed to be energy independent. There is a small variation in σ_j ($\approx$20 percent) which must eventually be taken into account. Solving equation (5.16) by using line integration with an integrating factor

$$\mu_j(\eta_j, \xi_j) = \exp\left[\frac{1}{2}\sigma_j(\xi_j + \eta_j)\right] \tag{5.17}$$

results in

$$\chi_j(\eta_j, \xi_j) = \exp\left[-\frac{1}{2}\sigma_j(\xi_j + \eta_j)\right]\ \chi_j(-\xi_j, \xi_j) + \frac{1}{2}\int_{-\xi_j}^{\eta_j} \exp\left[\frac{1}{2}\sigma_j(\eta' - \eta_j)\right] \sum_k\ m_{jk}\sigma_k \frac{\nu_j}{\nu_k}\ \chi_k(\eta'_k, \xi'_k)\ d\eta' \tag{5.18}$$

where

$$\eta'_k = \frac{\nu_k\ +\ \nu_j}{2\nu_k}\eta' + \frac{\nu_k\ -\ \nu_j}{2\nu_k}\xi_j$$

and

$$\xi'_k = \frac{\nu_k\ -\ \nu_j}{2\nu_k}\eta' + \frac{\nu_k\ +\ \nu_j}{2\nu_k}\xi_j$$

Defining

$$\psi_j(x, r_j) = \chi_j(\eta_j, \xi_j) \tag{5.19}$$

one may show

$$\psi_j(x, r_j) = \exp(-\sigma_j x)\psi_j(0, r_j + x) + \int_0^x dz\ \exp(-\sigma_j z) \sum_k\ m_{jk}\sigma_k \frac{\nu_j}{\nu_k}\ \psi_k\left(x - z, r_k + \frac{\nu_j}{\nu_k}z\right) \tag{5.20}$$

Furthermore, it is easy to show that

$$\psi_j(x+h,r_j) = \exp(-\sigma_j h)\ \psi_j(x,r_j+h) + \int_0^h dz\ \exp(-\sigma_j z) \sum_k\ m_{jk}\sigma_k \frac{\nu_j}{\nu_k}\ \psi_k\left(x+h-z, r_k + \frac{\nu_j}{\nu_k} z\right) \tag{5.21}$$

It is clear from equation (5.20) that

$$\psi_k(x+h-z,r_k) = \exp[-\sigma_k(h-z)]\ \psi_k(x,r_k+h) + O(h-z) \tag{5.22}$$

which upon substitution into equation (5.21) yields

$$\psi_j(x+h,r_j) = \exp(-\sigma_j h)\ \psi_j(x,r_j+h) + \int_0^h dz\ \exp(-\sigma_j z) \sum_k\ m_{jk}\sigma_k \frac{\nu_j}{\nu_k}\ \exp[-\sigma_k(h-z)]\ \psi_k\left(x, r_k + \frac{\nu_j}{\nu_k} z + h - z\right) \tag{5.23}$$

which is correct to order h^2. This expression may be further approximated by

$$\psi_j(x+h,r_j) = \exp(-\sigma_j h)\ \psi_j(x,r_j+h) + \sum_k\ m_{jk}\sigma_k \frac{\nu_j}{\nu_k} \left[\frac{\exp(-\sigma_j h) - \exp(-\sigma_k h)}{\sigma_k - \sigma_j}\right] \psi_k\left(x, r_k + \frac{\nu_j}{\nu_k} h\right) \tag{5.24}$$

which is accurate to $O\left[(\nu_k - \nu_j)\, h\right]$. Equation (5.24) is the basis of the Galactic Cosmic Rays (GCR) Transport Code GCRTRN (Wilson and Badavi 1986; Wilson, Townsend, and Badavi 1987a; Wilson and Townsend 1988). The nucleon transport equation (4.2) is solved by adding the heavy ion collision source of nucleons to the BRYNTRN code (Wilson et al. 1989).

There are several quantities of interest that are now given. The integral fluence is given as

$$\phi_j(x,>E) = \int_{R_j(E)}^{\infty} \psi_j(x,r)\ dr \tag{5.25}$$

The energy absorption per gram is

$$D_j(x,>E) = \int_E^{\infty} A_j \psi_j[x, R_j(E)]\ dE \tag{5.26}$$

with the dose equivalent given as

$$H_j(x,>E) = A_j \int_E^{\infty} Q_F\ \psi_j[x, R_j(E)]\ dE \tag{5.27}$$

These quantities are used in shield design studies for protection against galactic cosmic rays.

6. Analytic Benchmarks

In this section, we address the question of GCR transport code validation. Ideally, validation should be accomplished with detailed transport data obtained from carefully planned and controlled experiments; unfortunately, there exists a paucity of such data. Although useful for comparison purposes, the atmospheric propagation measurements used previously (Wilson, Townsend, and Badavi 1987a) are clearly not definitive because they consist of integral fluences

of as many as 10 different nuclear species combined into a single datum. Although limited quantities of HZE dosimetry measurements from manned space missions (e.g., Skylab) are also available (Benton, Henke, and Peterson 1977), numerous assumptions concerning the relationships between dosimeter locations and spacecraft shield thicknesses and geometry must be made to estimate astronaut doses with GCR codes. Because many of these assumptions may involve inherently large uncertainties (a factor of 2 or greater), it becomes difficult to attribute any differences to particular assumptions or approximations that may have been used in the analyses. Without definitive GCR transport measurements with which to compare code predictions, other methods of validation must be considered. As noted by Wilson (1983) and Wilson et al. (1989a), there are several different versions of HZE transport codes available. When used with the same input spectra, interaction parameters, and boundary conditions, all should yield comparable results. The history of transport code development, however, suggests otherwise. For this reason, a realistic, nontrivial, exact, analytic solution to the simplified Boltzmann equation used to describe HZE transport has been formulated as an absolute standard for code comparison purposes.

For the benchmark problem, the incident spectrum is limited to a single ion type ($j = J$). Because the GCR spectrum for a typical ion is of the form

$$F(E) \sim E^{-\alpha} \tag{6.1}$$

where $\alpha \approx 2.5$, we choose the energy spectrum to be of similar functional form as

$$F_j(E) = \frac{\delta_{jJ}}{[R_J(E)]^2}\ \widetilde{S}_j(E) \tag{6.2}$$

Defining the characteristic variables as

$$\eta_j = x - R_j(E) \tag{6.3}$$

and

$$\xi_j = x + R_j(E) \tag{6.4}$$

equation (5.1) can be solved by the method of characteristics (Wilson 1977a; Wilson, et al. 1989) to give

$$\psi_J(x,E) = \frac{\exp(-\hat{\sigma}_J x)}{[\nu_J x + R_J(E)]^2} \tag{6.5}$$

where

$$\psi_J(x,E) \equiv \widetilde{S}_j(E)\ \phi_J(x,E) \tag{6.6}$$

and

$$\hat{\sigma}_J = \sigma_J(1 - m_{JJ}) \tag{6.7}$$

This is the trivial solution for the incident beam species. For $j < J$ (secondary fragments), it can be shown that

$$\psi_j(x,E) = \sigma_J m_{jJ}\ \frac{\nu_j}{\nu_J}\ I_j(x,E)\ \exp\left[\frac{-(\hat{\sigma}_j\eta_j + \hat{\sigma}_J\ \xi_j)}{2}\right] \tag{6.8}$$

where in terms of the exponential integral function $E_2(x)$ (see Abramowitz and Stegun 1964),

$$I_j(x,E) = \frac{\exp[-b(\nu_J + \nu_j)\xi_j/2]}{\nu_J - \nu_j}\left[\frac{E_2(b\nu_j\xi_j)}{\nu_j\xi_j} - \frac{E_2(b\nu_J\xi_J)}{\nu_J\xi_J}\right] \tag{6.9}$$

for $j = J - 1$ and

$$b = \frac{\hat{\sigma}_J - \hat{\sigma}_j}{\nu_J - \nu_j} \tag{6.10}$$

Clearly, equations (6.9) and (6.10) are true for all j if $m_{kj} = 0$ for all values of $j < J$ (i.e., if the secondary fragments themselves do not fragment).

The benchmark solution was calculated for an incident iron beam ($J = 26$) in an aluminum target, for which the input parameters are $\hat{\sigma}_{26} = 0.04568$ cm^2/g, $\hat{\sigma}_{25} = 0.04260$ cm^2/g, and $m_{25,26}\ \sigma_{26} = 0.00403$ cm^2/g. Results of the GCR transport code simulation of this benchmark for the propagating incident iron beam and secondary manganese ($j = 25$) ions and the exact analytic predictions obtained from equations (6.5) and (6.8) are given in tables 6.1 and 6.2. It is clear from these tabulated results that the numerical solution methods developed previously (Wilson and Badavi 1986; Wilson, Townsend, and Badavi 1987a) are accurate in solving equation (5.1) for GCR transport to within about 1 percent. This indicates that any limitations to accurately solving GCR transport problems must focus upon the simplifying approximations used to obtain equation (5.1) as well as upon unresolved issues concerning the need to include multiple coulomb scattering effects, fragment momentum dispersion effects, and perhaps most important, the nature and quality of the input cross-section data bases. To illustrate this point, we are aware of only one heavy ion transport code (Wilson et al. 1984), which uses energy-dependent cross sections. Recent studies, however, suggest that fully energy-dependent cross sections may be important for some transport code applications (Townsend and Wilson 1988).

Table 6.1. Benchmark Numerical Simulation and Analytic Solution for Iron Ions as Function of Ion Depth[a] and Energy Into Aluminum Absorber

E, MeV/amu	$\psi_{\mathrm{Fe}}(0, E)$		$\psi_{\mathrm{Fe}}(10, E)$		$\psi_{\mathrm{Fe}}(20, E)$	
	Numerical	Analytic	Numerical	Analytic	Numerical	Analytic
0.0198	1.394×10^{5}	1.394×10^{5}	4.334×10^{-5}	4.382×10^{-5}	6.942×10^{-6}	7.044×10^{-6}
0.1147	1.692×10^{4}	1.692×10^{4}	4.334×10^{-5}	4.381×10^{-5}	6.942×10^{-6}	7.044×10^{-6}
1.090	9.217×10^{2}	9.217×10^{2}	4.333×10^{-5}	4.379×10^{-5}	6.942×10^{-6}	7.043×10^{-6}
10.07	1.062×10^{1}	1.062×10^{1}	4.321×10^{-5}	4.360×10^{-5}	6.932×10^{-6}	7.027×10^{-6}
100.1	9.310×10^{-3}	9.310×10^{-3}	3.699×10^{-5}	3.718×10^{-5}	6.400×10^{-6}	6.478×10^{-6}
1 059	5.089×10^{-6}	5.089×10^{-6}	2.014×10^{-6}	2.019×10^{-6}	8.741×10^{-7}	8.799×10^{-7}
10 490	2.970×10^{-8}	2.970×10^{-8}	1.833×10^{-8}	1.833×10^{-8}	1.132×10^{-8}	1.132×10^{-8}

[a]Depth is given in g/cm^2.

Table 6.2. Benchmark Numerical Simulation and Analytic Solution for Secondary Manganese Ions as Function of Ion Depth[a] and Energy Into Aluminum Absorber

E, MeV/amu	$\psi_{\mathrm{Mn}}(10, E)$		$\psi_{\mathrm{Mn}}(20, E)$	
	Numerical	Analytic	Numerical	Analytic
0.0198	1.772×10^{-6}	1.780×10^{-6}	5.704×10^{-7}	5.768×10^{-7}
0.1147	1.772×10^{-6}	1.780×10^{-6}	5.704×10^{-7}	5.768×10^{-7}
1.090	1.772×10^{-6}	1.779×10^{-6}	5.704×10^{-7}	5.767×10^{-7}
10.07	1.767×10^{-6}	1.771×10^{-6}	5.696×10^{-7}	5.753×10^{-7}
100.1	1.504×10^{-6}	1.503×10^{-6}	5.242×10^{-7}	5.219×10^{-7}
1 059	7.797×10^{-8}	7.806×10^{-8}	6.880×10^{-8}	6.918×10^{-8}
10 490	7.004×10^{-10}	7.004×10^{-10}	8.728×10^{-10}	8.728×10^{-10}

[a]Depth is given in g/cm^2.

7. High Charge and Energy (HZE) Nuclear Data Base

The nuclear cross sections for neutron and proton interactions are described extensively by Wilson et al. (1989a and 1989b). The heavy ion absorption cross sections σ_{abs} are currently derived from

$$\sigma_{\text{abs}}(A_P, A_T) = \pi r_o^2 \left[A_p^{1/3} + A_T^{1/3} - 0.4\right]^2 \tag{7.1}$$

which was fit to the asymptotic nuclear cross sections calculated by Wilson and Townsend (1981).

In the abrasion-ablation fragmentation model, the projectile nuclei, moving at relativistic speeds, collide with stationary target nuclei. In the abrasion step, those portions of the nuclear volumes that overlap are sheared away by the collision. The remaining projectile piece, called a prefragment or primary residue, continues its trajectory with essentially its precollision velocity. As a result of the dynamics of the abrasion process, the prefragment is highly excited and subsequently decays by the emission of gamma radiation and/or nuclear particles. This step is the ablation stage. The resultant isotope, sometimes referred to as a secondary product, is the nuclear fragment whose cross section is measured. The abrasion process can be analyzed with classical geometric arguments (Bowman, Swiatecki, and Tsang 1973) or methods obtained from formal quantum scattering theory (Townsend et al. 1986a and 1986b). The ablation stage can be analyzed from geometric arguments (Bowman, Swiatecki, and Tsang 1973) or more sophisticated methods based upon Monte Carlo or intranuclear cascade techniques (Gosset et al. 1977; Hüfner, Schäfer, and Schürmann 1975; Morrissey et al. 1978; Guthrie 1970). Predictions of fragmentation cross sections can also be made with the approximate semiempirical parameterization formulas of Silberberg, Tsao, and Shapiro (1976) and Silberberg, Tsao, and Letaw (1983).

The amount of nuclear material stripped away in the collision of two nuclei of radius R_P and R_T is taken as the volume of overlap region times an average attenuation factor. The relevant formula for the constituents in the overlap volume in the projectile is given by the following formula:

$$\Delta_{\text{abr}} = F A_P \left[1 - \frac{1}{2}\exp\left(\frac{-C_P}{\lambda}\right) - \frac{1}{2}\exp\left(\frac{-C_T}{\lambda}\right)\right] \tag{7.2}$$

where C_P and C_T are the maximum chord lengths of the intersecting surface in the projectile and the target, respectively, λ is the nuclear mean free path, and the expressions for F differ depending on the nature of the collision (peripheral versus central) and the relative sizes of the colliding nuclei.

For $R_T > R_P$, we have (Gosset et al. 1977)

$$\begin{aligned} P = {} & 0.125(\mu\nu)^{1/2}\left(\frac{1}{\mu} - 2\right)\left(\frac{1-\beta}{\nu}\right)^2 \\ & - 0.125\left[0.5(\mu\nu)^{1/2}\left(\frac{1}{\mu} - 2\right) + 1\right]\left(\frac{1-\beta}{\nu}\right)^3 \end{aligned} \tag{7.3}$$

and

$$\begin{aligned} F = {} & 0.75(1-\nu)^{1/2}\left(\frac{1-\beta}{\nu}\right)^2 \\ & - 0.125\left[3(1-\nu)^{1/2} - 1\right]\left(\frac{1-\beta}{\nu}\right)^3 \end{aligned} \tag{7.4}$$

with

$$\nu = \frac{R_P}{R_P + R_T} \tag{7.5}$$

$$\beta = \frac{b}{R_P + R_T} \tag{7.6}$$

and

$$\mu = \frac{1}{\nu} - 1 = \frac{R_T}{R_P} \tag{7.7}$$

Equations (7.3) and (7.4) are valid when the collision is peripheral (i.e., the two nuclear volumes do not completely overlap). In this case, the impact parameter b is restricted such that

$$R_T - R_P \leq b \leq R_T + R_P \tag{7.8}$$

If the collision is central, then the projectile nucleus volume completely overlaps the target nucleus volume ($b < R_T - R_P$), and all the projectile nucleons are abraded. In this case, equations (7.3) and (7.4) are replaced by

$$P = -1 \tag{7.9}$$

and

$$F = 1 \tag{7.10}$$

and there is no ablation of the projectile because it was destroyed by the abrasion.

For the case where $R_P > R_T$ and the collision are peripheral, equations (7.3) and (7.4) become (Morrissey et al. 1978)

$$\begin{aligned} P = {} & 0.125(\mu\nu)^{1/2}\left(\frac{1}{\mu} - 2\right)\left(\frac{1-\beta}{\nu}\right)^2 \\ & - 0.125\left\{0.5\left(\frac{\nu}{\mu}\right)^{1/2}\left(\frac{1}{\mu} - 2\right)\frac{[(1/\nu)(1-\mu^2)^{1/2} - 1][(2-\mu)\mu]^{1/2}}{\mu^3}\right\} \\ & \times \left(\frac{1-\beta}{\nu}\right)^3 \end{aligned} \tag{7.11}$$

and

$$F = 0.75(1-\nu)^{1/2}\left(\frac{1-\beta}{\nu}\right)^2 - 0.125\left\{\frac{3(1-\nu)^{1/2}}{\mu} - \frac{[1-(1-\mu^2)^{3/2}][1-(1-\mu)^2]^{1/2}}{\mu^3}\right\}\left(\frac{1-\beta}{\nu}\right)^3 \tag{7.12}$$

where the impact parameter is restricted such that

$$R_P - R_T \leq b \leq R_P + R_T \tag{7.13}$$

For a central collision ($b < R_P - R_T$) with $R_P > R_T$, equations (7.11) and (7.12) become

$$P = \left[\frac{1}{\nu}(1-\mu^2)^{1/2} - 1\right]\left[1 - \left(\frac{\beta}{\nu}\right)^2\right]^{1/2} \tag{7.14}$$

and

$$F = \left[1 - (1-\mu^2)^{3/2}\right]\left[1 - \left(\frac{\beta}{\nu}\right)^2\right]^{1/2} \tag{7.15}$$

The charge ratio of removed nuclear matter is assumed to be that of the parent nucleus.

The surface distortion excitation energy of the projectile prefragment following abrasion of m nucleons is calculated from the clean-cut abrasion formalism of Bowman, Swiatecki, and Tsang (1973). For this model, the colliding nuclei are assumed to be uniform spheres of radii R_i ($i = P, T$). In collision, the overlapping volumes shear off so that the resultant projectile prefragment is a sphere with a cylindrical hole gouged out of it. The excitation energy is then determined by calculating the difference in surface area between the misshapen sphere and a perfect sphere of equal volume. This excess surface area ΔS is given by Gosset et al. (1977) as

$$\Delta S = 4\pi R_p^2[1 + P - (1 - F)^{2/3}] \tag{7.16}$$

where the expressions for P and F differ depending upon the nature of the collision (peripheral versus central) and the relative sizes of the colliding nuclei which were given in previous equations.

The excitation energy associated with surface energy is known to be 0.95 MeV/fm^2 for near equilibrium nuclei so that

$$E_s' = 0.95\ \Delta S \tag{7.17}$$

for small surface distortions. When large numbers of nucleons are removed in the abrasion process, equation (7.17) is expected to be an underestimate of the actual excitation. We therefore introduce an excess excitation factor in terms of the number of abraded nucleons $\Delta_{\rm abr}$ as

$$f = 1 + \frac{10\Delta_{\rm abr}}{A_P} + \frac{25\Delta_{\rm abr}^2}{A_P^2} \tag{7.18}$$

which approaches 1 when the impact parameter is large but increases the excess excitation when many nucleons are removed in the collisions and when grossly misshapened nuclei are formed. The total excitation energy is then

$$E_s = E_s' f \tag{7.19}$$

which reduces to equation (7.17) for small $\Delta_{\rm abr}$. We assume that all fragments with a mass of 5 are unbound, 90 percent of the fragments with a mass of 8 are unbound, and 50 percent of fragments with a mass of 9 (^{9}B) are unbound.

A secondary contribution to the excitation energy is the transfer of kinetic energy of relative motion across the intersecting boundary of the two ions. The rate of energy loss of a nucleon when it passes through nuclear matter (Westfall et al. 1979) is taken at 13 MeV/fm, and the energy deposit is assumed to be symmetrically dispersed about the azimuth so that 6.5 MeV/fm per nucleon at the interface is the average rate of energy transfer into excitation energy. This energy is transferred in single particle collision processes, and the energy is transferred to excitation energy of the projectile for half of the events and leaves the projectile excitation energy unchanged for the remaining half of the events. The first estimate of this contribution is to use the length of the longest chord C_1 in the projectile surface interface. This chord length is the maximum distance traveled by any target constituent through the projectile interior. The number of other target constituents in the interface region may be found by estimating the maximum chord C_t transverse to the projectile velocity which spans the projectile surface interface. The total excitation energy from excess surface and spectator interaction is then

$$E_x' = 13C_1 + \frac{1}{3}13C_1(C_t - 1.5) \tag{7.20}$$

where the second term only contributes if $C_t > 1.5$ fm. We further assume that the effective longitudinal chord length for these remaining nucleons is one third the maximum chord length.

The decay of highly excited nuclear states is dominated by heavy particle emission. In the present model, we assume a nucleon is removed for every 10 MeV of excitation energy as

$$\Delta_{\text{abl}} = \frac{E_s + E_x}{10 \text{ MeV}} \tag{7.21}$$

In accordance with the previously discussed directionality of the energy transfer, E_x has two values as

$$E_x = \left\{ \begin{array}{ll} E'_x & \left(P_x = \frac{1}{2}\right) \\ 0 & \left(P_{\bar{x}} = \frac{1}{2}\right) \end{array} \right\} \tag{7.22}$$

where P_j is the corresponding probability of occurrence of each value in collisions.

The number of nucleons removed through the abrasion-ablation process is given as a function of impact parameter as

$$\Delta A = \Delta_{\text{abr}}(b) + \Delta_{\text{abl}}(b) \tag{7.23}$$

The values of ΔA for carbon projectiles on a copper target and for copper projectiles on a carbon target are shown in figure 7.1. For each projectile, the dashed curve corresponds to $E_x = 0$, whereas the solid curve corresponds to $E_x = E'_x$ as given by equation (7.20). A real collision would be given by a statistical distribution between the limits shown by these two curves. The average event is calculated as if the two extremes occurred with equal probability, as noted in equations (7.22).

The nuclear fragmentation parameters herein are approximated according to the abrasion-ablation model of Bowman, Swiatecki, and Tsang (1973). The cross section for removal of ΔA nucleons is estimated as

$$\sigma(\Delta A) = \pi b_2^2 - \pi b_1^2 \tag{7.24}$$

where b_2 is the impact parameter for which the volume of intersection of the projectile contains Δ_{abr} nucleons and the resulting excitation energies release an additional Δ_{abl} nucleons at the rate of 1 nucleon for every 10 MeV of excitation such that

$$\Delta_{\text{abr}}(b_2) + \Delta_{\text{abl}}(b_2) = \Delta A - \frac{1}{2} \tag{7.25}$$

and similarly for b_1

$$\Delta_{\text{abr}}(b_1) + \Delta_{\text{abl}}(b_1) = \Delta A + \frac{1}{2} \tag{7.26}$$

The charge distributions of the final projectile fragments are strongly affected by nuclear stability. We expect that the Rudstam (1966) charge distribution for a given $\sigma(\Delta A)$ to be reasonably correct as

$$\sigma(A_F, Z_F) = F_1 \exp\left(-R|Z_F - SA_F + TA_F^2|^{3/2}\right) \sigma(\Delta A) \tag{7.27}$$

where $R = 11.8/A_F^D$, $D = 0.45$, $S = 0.486$, and $T = 3.8 \times 10^{-4}$ according to Rudstam and F_1 is a normalizing factor such that

$$\sum_{Z_F} \sigma(A_F, Z_F) = \sigma(\Delta A) \tag{7.28}$$

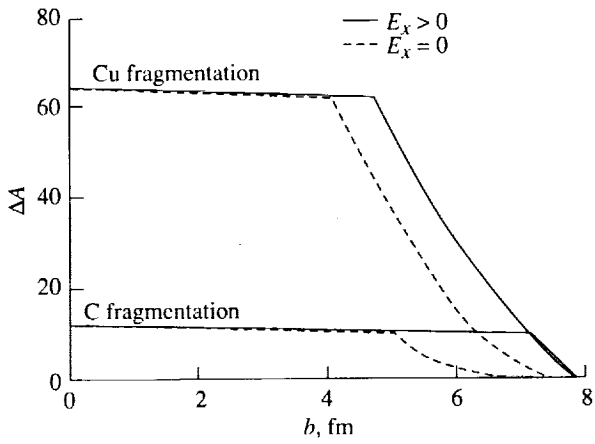

Figure 7.1. Nucleon removal number as function of impact parameter in carbon-copper collisions.

The Rudstam formula for $\sigma(\Delta A)$ was not used because the ΔA dependence is too simple and breaks down for heavy targets (Townsend et al. 1984; Townsend, Wilson, and Norbury 1985).

The charge of the removed nucleons ΔZ is calculated according to charge conservation

$$Z_P = Z_F + \Delta Z \tag{7.29}$$

and is divided among the nucleons and alpha particles according to the following rules. The abraded nucleons are those removed from that portion of projectile in the overlap region with the target. Therefore, the abraded nucleon charge is assumed to be proportional to the charge fraction of the projectile nucleus as

$$Z_{\text{abr}} = \frac{Z_P \Delta_{\text{abr}}}{A_P} \tag{7.30}$$

This, of course, ignores the charge separation caused by the giant dipole resonance model of Morrissey et al. (1978). The charge release in the ablation is then given as

$$Z_{\text{abl}} = \Delta Z - Z_{\text{abr}} \tag{7.31}$$

which simply conserves the remaining charge.

The alpha particle is known to be unusually tightly bound in comparison with other nucleon arrangements. Because of this usually tight binding of the alpha particle, the helium production is maximized in the ablation process

$$N_\alpha = \text{int}\left(\frac{Z_{\text{abr}}}{2}\right) \tag{7.32}$$

where $\text{int}(x)$ denotes the integer part of x. The number of protons produced is given by charge conservation as

$$N_P = \Delta Z - 2N_\alpha \tag{7.33}$$

Similarly, neutral conservation requires the number of neutrons produced to be

$$N_n = \Delta A - N_p - 4N_\alpha \tag{7.34}$$

The fragments with masses of 2 and 3 are ignored.

The calculation is performed for $\Delta A = 1$ to $\Delta A = A_P - 1$, for which the cross section associated with $\Delta A > A_P - 0.5$ is missed. These are, of course, the central collisions for which the projectile is assumed to disintegrate into single nucleons if $R_P < R_T$ as

$$N_P = Z_P \tag{7.35}$$

$$N_n = A_P - Z_P \tag{7.36}$$

and is ignored otherwise. The energetic target fragments are being ignored as well as the mesonic components. The peripheral collisions with $\Delta A < 0.5$ are also missing. Most important in these near collisions is the coulomb dissociation process studied by Norbury and Townsend (1986).

Only the nuclear radius for use in the model is yet undefined. Equation (7.1) is an accurate representation of the high-energy cross sections. The choice of nuclear radius as

$$R = 1.26A^{1/3} \tag{7.37}$$

is consistent with equation (7.1) for $r_0 = 1.26$ fm when the peripheral collisions ($\Delta A < 0.5$) are taken into account. This completes the description of the basic fragmentation model in present use.

In the present evaluation, we look only to elemental fragmentation cross sections for which most of the experimental data have been obtained. This is also motivated by the crudeness of the present model which is not expected to be completely accurate. Even so, the quality of the experimental data base is uncertain with experiments of different groups differing by a factor of 2, in general, and even more for specific isotopes.

The first comparison is with the experiments of Heckman (1975) with ^{12}C ion beams at 1.05 GeV/amu on the series of targets extending from hydrogen to lead as shown in table 7.1. The present calculations are shown as values in parentheses. The calculated values for hydrogen targets are those of Rudstam (1966). Note that all values are within 20 percent of the experiments with few exceptions (namely, fragments from hydrogen targets and the neutron removal cross section in copper and lead targets).

The charge removal cross sections for several projectiles on carbon targets are given in table 7.2. The agreement between the present model and the Lawrence Berkeley Laboratory groups (Heckman 1975; Westfall et al. 1979) is quite good. Our results tend to be low compared with the experiments of Webber et al. (1983a and 1983b) and Guerreau et al. (1983). The model can be adjusted once experimental differences are resolved.

The elemental fragmentation cross section of iron projectiles on several targets is shown in table 7.3. Again, reasonable agreement is found generally throughout the table with a few examples of relatively large errors. The quantities in brackets at the bottom of the table are the coulomb dissociation cross sections for forming manganese. These are to be added to the nuclear fragmentation cross sections for manganese in parentheses before comparing with experimental values.

Table 7.1. Fragmentation Cross Sections of Carbon Beams at 1.05 GeV/amu in Various Targets

[Quantities in parentheses are present theory]

Fragment	Carbon cross section,[a] mb, in target of—				
	H (b)	Be	C	Cu	Pb
Li	23 ± 2 (34)	51 ± 2 (54)	52 ± 3 (61)	71 ± 5 (81)	103 ± 14 (113)
Be	17 ± 1 (22)	35 ± 1 (32)	35 ± 1 (33)	47 ± 2 (48)	71 ± 6 (63)
B	50 ± 4 (42)	81 ± 4 (86)	78 ± 3 (100)	119 ± 8 (138)	203 ± 32 (185)
C	28 ± 3 (10)	49 ± 3 (39)	50 ± 4 (44)	86 ± 8 (57)	139 ± 22 (79)

[a]Heckman 1975.

[b]Values in parentheses in this column are those of modified Rudstam (1966).

Table 7.2. Charge Removal Cross Sections of Various Projectiles on Carbon Targets

[Quantities in parentheses are present theory; number in brackets is energy in GeV/amu]

ΔZ	Charge removal cross section, mb, of projectile of					
	C [2.1] (a)	O [2.1] (a)	O [0.9] (b)	Ne [0.47] (b)	Ar [0.21] (c)	Fe [1.88] (d)
0	50 ± 4 (40)	45 ± 2 (45)	-----	----- (40)	------ (132)	------- (64)
1	78 ± 3 (100)	105 ± 4 (101)	176 ± 5	129 ± 3 (90)	--- (151)	181 ± 27 (157)
2	35 ± 1 (33)	116 ± 6 (93)	164 ± 5	214 ± 3 (98)	154 ± 26 (85)	124 ± 13 (110)
3	52 ± 2 (61)	50 ± 2 (65)	55 ± 3	155 ± 3 (75)	122 ± 16 (72)	100 ± 11 (87)
4		36 ± 1 (24)	27 ± 2	140 ± 3 (65)	144 ± 19 (64)	87 ± 11 (76)
5		65 ± 3 (47)	------	74 ± 2 (54)	81 ± 15 (59)	54 ± 9 (62)
6				33 ± 1 (19)	112 ± 15 (51)	78 ± 11 (67)
7				----- (40)	90 ± 3 (50)	52 ± 7 (57)
8					92 ± 13 (44)	55 ± 9 (52)
9					65 ± 11 (42)	53 ± 7 (49)
10					83 ± 13 (37)	54 ± 10 (45)
11					------ (35)	59 ± 10 (42)
12						57 ± 10 (39)
13						83 ± 11 (36)
14						------ (35)

[a]Heckman 1975.

[b]Webber et al. 1983a and 1983b.

[c]Guerreau et al. 1983.

[d]Westfall et al. 1979.

Comparing the model cross sections with the experimental data set reveals that 92 percent of the calculated cross sections are within 50 percent of the measured values. If we reduce the error band to 30 percent, we will find 81 percent of the cross sections are in agreement to within this level. Among the least accurate are the ion on hydrogen target data which again is Rudstam's theory and the cross sections of Webber et al. Note that our model agrees with experiments to the extent that the experimentalists agree among themselves for the same projectile-target combinations. From this point of view, little progress can be made in improving the model until the experimental situation is clarified. The model of Silberberg, Tsao, and Shapiro (1976), which includes many corrections to Rudstam's formulas, is preferred for hydrogen targets.

Table 7.3. Fragmentation Cross Section of Iron Projectiles at 1.88 GeV/amu in Various Targets

[Quantities in parentheses are values from present model; values in brackets at bottom of table are coulomb dissociation cross sections for forming manganese]

	Cross section, mb, of iron projectiles in—									
Z_F	H (a)	Li	Be	C	S	Cu	Ag	Ta	Pb	U
13	25 ± 10 (19)	50 ± 5 (33)	50 ± 7 (34)	83 ± 11 (36)	78 ± 18 (45)	179 ± 27 (57)	112 ± 19 (64)	81 ± 14 (72)	191 ± 34 (74)	307 ± 79 (77)
14	31 ± 9 (22)	54 ± 5 (36)	75 ± 8 (37)	57 ± 10 (39)	106 ± 14 (47)	72 ± 11 (61)	158 ± 20 (67)	115 ± 20 (75)	119 ± 22 (77)	169 ± 28 (80)
15	22 ± 10 (26)	57 ± 6 (39)	57 ± 8 (38)	59 ± 10 (42)	50 ± 8 (51)	88 ± 15 (63)	64 ± 13 (70)	133 ± 20 (79)	78 ± 16 (81)	176 ± 34 (84)
16	37 ± 24 (30)	56 ± 6 (43)	63 ± 8 (45)	54 ± 10 (45)	74 ± 12 (54)	56 ± 11 (67)	96 ± 13 (74)	109 ± 17 (82)	116 ± 19 (85)	116 ± 22 (88)
17	36 ± 18 (36)	38 ± 4 (44)	54 ± 7 (48)	53 ± 7 (49)	66 ± 14 (58)	86 ± 13 (71)	79 ± 14 (79)	101 ± 18 (87)	90 ± 19 (90)	133 ± 22 (93)
18	31 ± 9 (41)	55 ± 6 (49)	54 ± 7 (51)	55 ± 9 (52)	74 ± 13 (62)	95 ± 15 (76)	84 ± 14 (83)	100 ± 18 (94)	73 ± 15 (95)	113 ± 19 (98)
19	36 ± 9 (47)	56 ± 5 (53)	65 ± 7 (55)	52 ± 7 (57)	55 ± 21 (66)	88 ± 14 (81)	79 ± 11 (89)	111 ± 20 (98)	90 ± 19 (101)	105 ± 15 (104)
20	47 ± 11 (55)	64 ± 6 (59)	68 ± 7 (60)	78 ± 11 (67)	97 ± 14 (72)	98 ± 14 (87)	118 ± 14 (96)	107 ± 17 (106)	144 ± 22 (109)	143 ± 19 (112)
21	62 ± 11 (65)	67 ± 6 (64)	77 ± 8 (66)	54 ± 9 (62)	91 ± 13 (79)	100 ± 15 (95)	104 ± 13 (104)	129 ± 18 (116)	111 ± 17 (118)	153 ± 21 (122)
22	22 ± 13 (77)	75 ± 6 (71)	83 ± 9 (74)	87 ± 11 (76)	64 ± 10 (89)	101 ± 14 (106)	124 ± 16 (116)	152 ± 19 (129)	148 ± 22 (132)	95 ± 16 (136)
23	60 ± 11 (88)	88 ± 7 (83)	88 ± 9 (84)	100 ± 11 (87)	86 ± 12 (103)	121 ± 15 (121)	117 ± 15 (132)	150 ± 19 (146)	142 ± 20 (151)	181 ± 27 (156)
24	80 ± 13 (101)	98 ± 7 (101)	111 ± 9 (105)	124 ± 13 (110)	128 ± 16 (126)	149 ± 16 (146)	218 ± 21 (161)	206 ± 22 (176)	242 ± 25 (181)	208 ± 22 (190)
25	127 ± 24 (119)	141 ± 18 (147)	156 ± 21 (154)	181 ± 27 (157)	250 ± 22 (182)	219 ± 20 (208)	280 ± 23 (228)	457 ± 34 (250)	509 ± 40 (256)	646 ± 43 (260)
	[0]	[1]	[1]	[3]	[15]	[42]	[97]	[211]	[258]	[316]

[a] Values in parentheses in this column are those of Rudstam (1966).

The semiempirical model for argon fragmentation on carbon is shown with the quantum mechanical optical model calculation (Townsend et al. 1986a) in figure 7.2. Also shown are experimental data of Viyogi et al. (1979). Reasonable agreement is seen between the two models except for neutron removal where there are no data yet to resolve the difference (Wilson, Townsend, and Badavi 1987b).

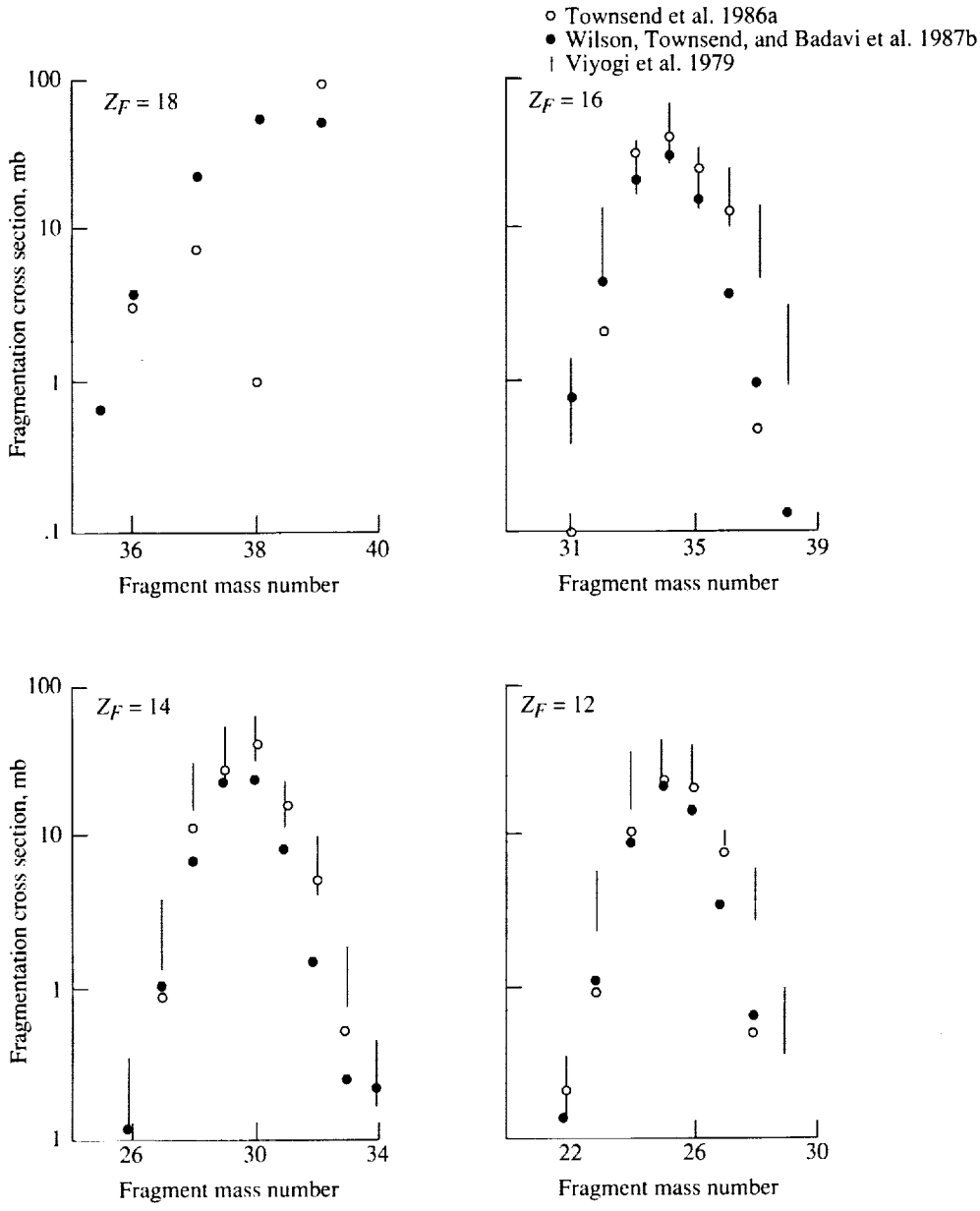

Figure 7.2. Representative argon-carbon fragmentation cross sections.

8. Space Radiation Exposure Issues

The differences in radiosensitivity of various tissues within an individual as well as individual differences are generally assumed to result from repair mechanisms (Curtis 1986; Fritz-Niggli 1988). The work of Swenberg, Holwitt, and Speicher (1990) suggests these differences may result from the structural state of the DNA as well. Repair also affects the dose response for protracted exposure. Current radiation protection guidelines use quality factors that are independent of dose rate (no time modifying factors), which may be of unusual importance in the small dose

rate exposures often experienced in space (NCRP 98 (Anon. 1989)). Clearly, well understood dose rate dependent models are needed (Curtis 1986; Anon. 1989). Furthermore, exposure received on a mission to the Moon or Mars will involve heavy ion exposure for which many issues concerning appropriate relative biological effectiveness (RBE) factors (hence, quality factors) are yet unknown. The accumulated levels of heavy ion exposure will be large and unprecedented in human experience (Nachtwey and Yang 1991). Although these issues may be studied in ground-based exposures with model biological systems, extrapolating to human exposure is difficult at best and space stress factors such as microgravity are unknown possible modifying factors in radiobiological response.

In addition to radiobiological response issues is the need to evaluate dose nonuniformity caused by body self-shielding (Khandelwal and Wilson 1974) and dose gradients within the shielding structure. For example, it is well known that tumor prevalence in the female breast is site specific even for relative uniform exposure (NCRP 85 (Anon. 1986)). We are led to believe that the exposure of only sensitive sites may be effective in tumor formation. Conversely, exposure of insensitive sites is assumed to be noneffective, and nonuniformity of exposure is a critical issue. In this section, we make some preliminary assessments concerning these issues and examine a limited number of shielding strategies to mitigate these radiation effects.

8.1. Galactic Cosmic Ray Exposure

The incident galactic cosmic ray spectrum (Adams, Silberberg, and Tsao 1981; Adams 1987) for free space is propagated through the target material by using the accurate analytical-numerical solutions to the transport equation described in chapter 10 of Wilson et al. 1991. These solution methods have been verified (to within 2 percent accuracy) by comparison with exact, analytical benchmark solutions to the ion transport equation (Wilson and Townsend 1988; Wilson et al. 1988).

These transport calculations include

1. Linear energy transfer (LET) dependent quality factors from ICRP 26 (Anon. 1977)
2. Dose contributions from propagating neutrons, protons, alpha particles, and heavy ions (high energy, high charge (HZE) particles)
3. Dose contributions resulting from target nuclear fragments, primary particles, and their secondaries
4. Dose contributions due to nuclear recoil in tissue

Major shortcomings of the calculations are as follows:

1. Except for tissue targets, contributions of fragments with masses of 2 and 3 are neglected
2. All secondary particles from HZE interactions are presently assumed to be produced with a velocity equal to that of the incident particle; this is conservative for neutrons produced in HZE particle fragmentations
3. Meson contributions to the propagating radiation fields are neglected
4. Nucleus-nucleus cross sections are not fully energy dependent (nucleon-nucleus cross sections are fully energy dependent)

These items are not conservative and probably alone result in a 15- to 30-percent underestimate of the exposure. As discussed by Townsend, Wilson, and Nealy (1989) and Townsend and Wilson (1988), the main sources of uncertainty are the input nuclear fragmentation model and the incident galactic cosmic ray (GCR) spectrum. Taken together, they could easily impose an uncertainty factor of 2 or more in the exposure predictions.

8.2. Results

In the present results, we use the ICRP 26 (Anon. 1977) quality factors which are currently in force within the U.S. space program. Figure 8.1 displays dose equivalent (in units of sieverts per year) as a function of water shield thickness (in units of areal density, grams per centimeter^2, or thickness, centimeters). Curves are displayed for solar minimum and solar maximum periods. For all thicknesses considered, the dose and dose equivalent during solar maximum are less than half the dose equivalent during solar minimum, at least according to the current estimates using the CREME environmental model of Adams (1987). Figure 8.2 displays results for dose and dose equivalent behind an aluminum shield. Also shown are measurements using the argon ion chambers at two shielded locations (Kovalev, Muratova, and Petrov 1989). The results for the location at 1 g/cm^2 are the most clear by experimental design. The mass distribution for the deeply shielded counter was poorly defined (Kovalev, Muratova, and Petrov 1989); this uncertainty is denoted in the figure by using parentheses around the data points. The solar maximum model predicted by CREME is clearly an underestimate. The solar minimum model appears in reasonable agreement with the Prognoz spacecraft data. Therefore, we will restrict the present analysis to solar minimum periods, which are the most limiting for GCR exposures. This does not imply, however, that exposures during solar maximum periods are not important. On the contrary, the cumulative exposures resulting from combined GCR and increased solar flare activity during solar maximum could potentially be significant (Nealy et al. 1990). During solar minimum periods, the estimated unshielded dose equivalent of 1.2 Sv does not exceed the exposure limits for either the skin or the ocular lens (which are 3 Sv for skin and 2 Sv for ocular lens). The dose equivalent at a depth of 5 cm, which yields an estimate of the exposure to the unshielded blood-forming organs (BFO), is 0.61 Sv, which exceeds the limit of 0.5 Sv by 22 percent. To reduce this estimated exposure below 0.5 Sv requires approximately 3.5 g/cm^2 (3.5 cm) of water shielding in addition to the body self-shielding of 5 g/cm^2 (5 cm).

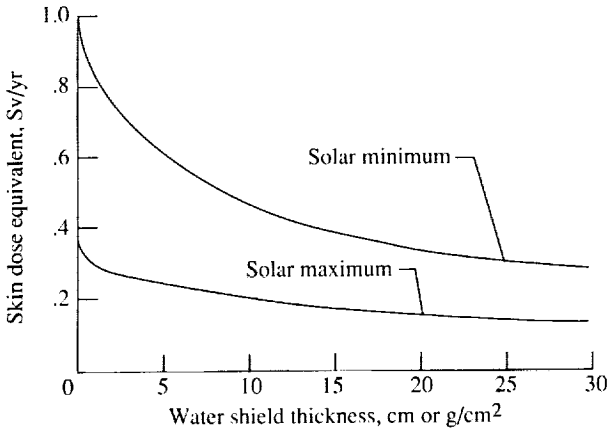

Figure 8.1. Dose equivalent resulting from galactic cosmic rays as function of water shield thickness.

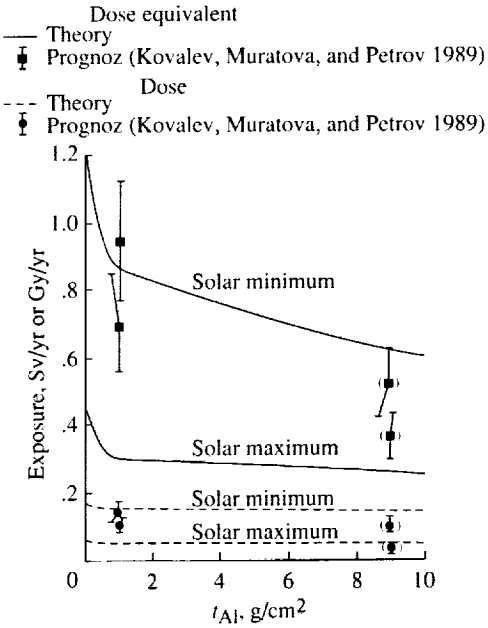

Figure 8.2. Deep space exposure behind aluminum shield. Parentheses denote depth in interior of Prognoz spacecraft.

For relative comparison purposes, the BFO dose equivalent as a function of shield thickness (areal density) is plotted in figure 8.3 for three materials (aluminum, water, and liquid hydrogen). Shielding effectiveness per unit mass increases as the composition of the shield changes from

heavier to lighter mass elements. For liquid hydrogen, an added advantage is the reduced neutron fluence caused by the absence of neutrons in the target composition and by the lack of target fragment contributions because of the elementary nature of hydrogen. From these results, for an allowed BFO exposure of 0.25 Sv/year, which corresponds to an uncertainty factor of 2 in a 0.5 Sv/year estimate, the mass ratios for the shielding are approximately 1:5:11 for LH_2:H_2O:Al. Obviously, for GCR shielding, the materials of choice are those composed of low atomic mass number constituents with significant hydrogen content.

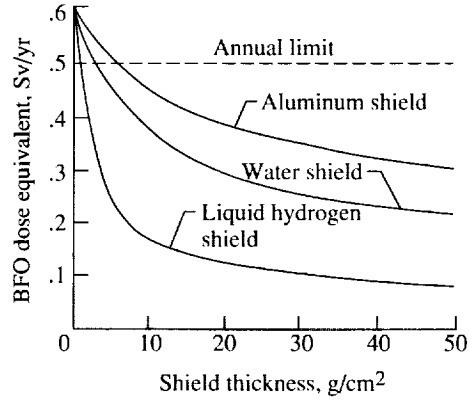

Figure 8.3. Dose equivalent in BFO as function of shield type and thickness.

Although the calculations are useful for estimating relative shield effectiveness to compare different materials, quantitatively the calculations should be considered as preliminary estimates of actual shield mass requirements. Aside from the previously mentioned shortcomings related to neglecting meson production and target fragment contributions from interactions of HZE particles and the target medium, figure 8.3 shows that the dose equivalent is a slowly decreasing function of shield thickness. This is a result of secondary particle production processes whereby the heavier GCR nuclei are broken into nucleons and lighter nuclear fragments by nuclear and coulombic interactions with the shield material. This slow decrease in dose equivalent with increasing shield thickness means that relatively small uncertainties in predicted doses arising from nuclear fragmentation model inaccuracies may yield large uncertainties in estimated shield thicknesses. A preliminary analysis of the nonlinear relationship between exposure uncertainty was presented by Townsend, Wilson, and Nealy (1989). The most startling finding was that an uncertainty factor of 2 in exposure amplified into an order of magnitude uncertainty in shield mass requirements.

8.3. Biological Effect Modifications

The rising RBE at low GCR dose results from the multitarget assumption in Katz theory leading to the sigmoid behavior in the survival curve of low-LET radiation as opposed to the exponential relationship for high-LET radiation (Cucinotta et al. 1991). The transition from sigmoid to exponential behavior is observed by Todd and Tobias (1974) to occur at 150 to 200 keV/μm for mammalian cells. Many also believe that the sigmoid behavior is related to repair mechanisms. This view is promoted by single exposure and split exposure experiments with a delay of 2.5 or 23 hours between fractions using V79 hamster cells as shown in figure 8.4 (Elkind and Sutton 1960). Repair is indicated by the sigmoid response of the second exposure after either the 2.5-hour repair period or especially the 23-hour repair period. Obviously the RBE based on such a photon exposure protocol depends on the history of the radiation induced damage. Similar survival studies with confluent C3H10T1/2 mouse cells (G1) indicate no repair for this end point for high-LET radiations (Yang et al. 1986). As a result of operative repair mechanisms (sparing) for low-LET exposure (fig. 8.5) and the lack of repair for high-LET

exposure (fig. 8.6), the corresponding RBE is dose rate dependent (Yang et al. 1986) as shown in figure 8.7. Also shown in figure 8.7 are the RBE values for neoplastic transformations. (Note, great liberty has been taken in connecting the data points.) The increase in RBE at low dose rate is in part indicative of repair of the damage for low-LET radiation (fig. 8.8) but additional enhancement of high-LET exposure at low dose rate (presumably some misrepair mechanism) also contributes for cell transformations (fig. 8.9). If misrepair/repair plays a role then this should be observed in the delayed plating experiments of Yang et al. (1989) as shown in figure 8.10. Instead the delayed plating experiments show no transformation misrepair but repair appears in cell survival data in distinction to the earlier low dose rate experiences with the same cell system.

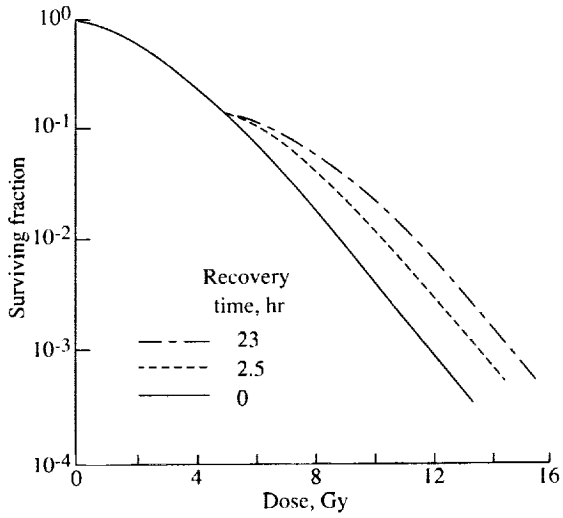

Figure 8.4. Fractional survival of cultured Chinese hamster cells for single exposure and exposure in two fractions (Elkind and Sutton 1960).

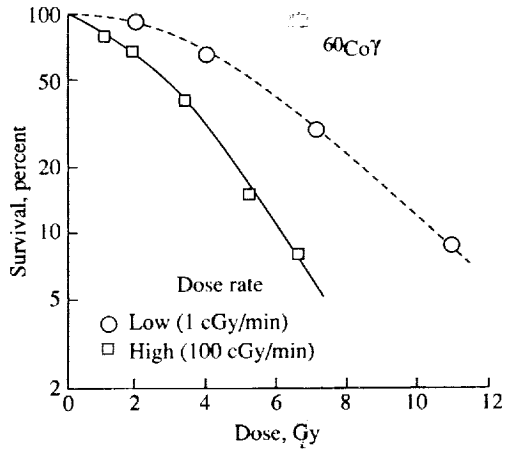

Figure 8.5. Survival fraction of confluent mouse cells at two dose rates displaying sparing at low dose rate (Yang et al. 1986).

Similar dose rate enhancement effects are observed in asynchronous cell cultures by Hill et al. (1982 and 1985, fig. 8.11) and whole animal exposures as observed by Thomson et al. (1981a and 1981b), Thomson, Williamson, and Grahn (1983, 1985a, 1985b, and 1986), and Thomson and Grahn (1988 and 1989) (fig. 8.12). These effects are considered the result of cell cycle phenomena (Rossi and Kellerer 1986; Brenner and Hall 1990). The basic model assumes that some phases of the cell cycle are more affected by radiation exposure. This is clearly seen in the cell synchronous experiments of Terasima and Tolmach (1963) shown in figure 8.13. The model of dose rate enhancement assumes only one cell phase is effective in injury of only that fraction in the sensitive phase. At a later time, a different fraction of cells is in the appropriate phase providing two exposed groups of cells and an apparent enhancement. Such a model was exploited in the work of Brenner and Hall (1990). This explanation fails to explain the enhancement effects observed by Yang et al. (1989) in cell transformation in stationary phase (G1) confluent C3H10T1/2.

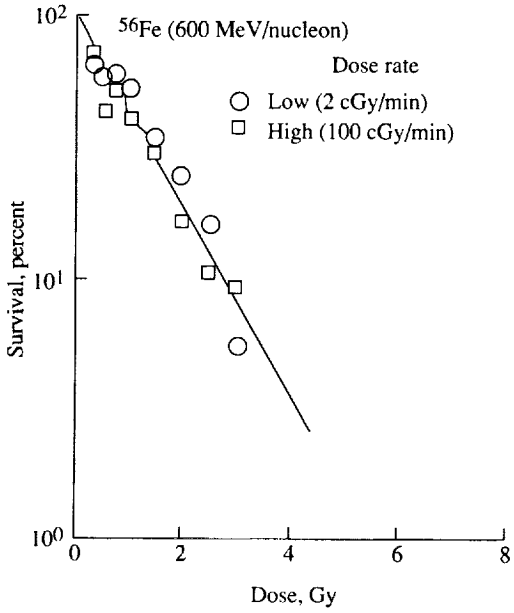

Figure 8.6. Dose rate effects on confluent mouse cell survival for high-LET exposure (Yang et al. 1986).

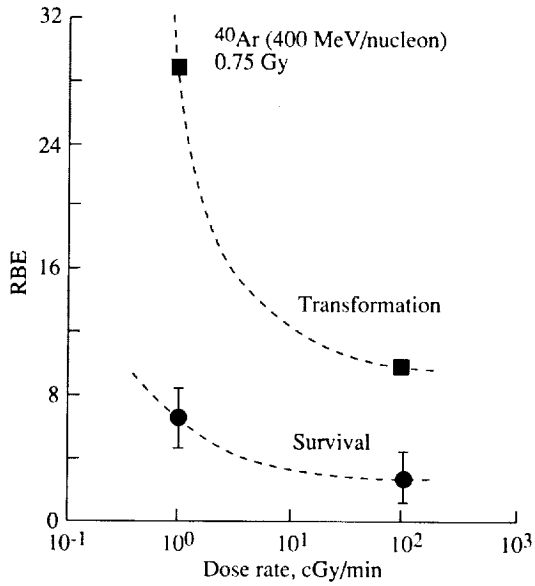

Figure 8.7. RBE as function of dose rate. The curves are to guide eye.

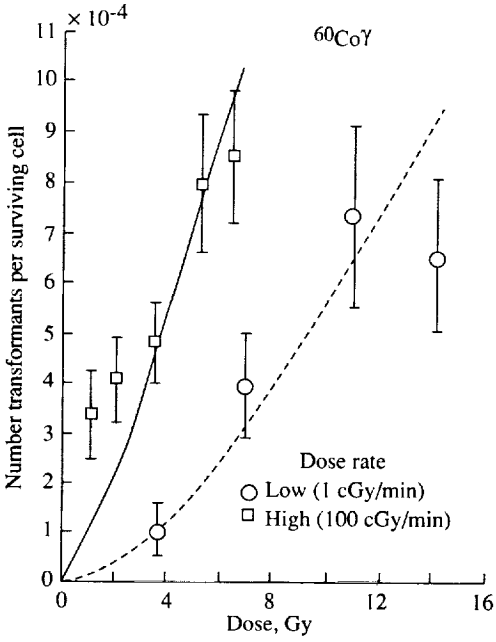

Figure 8.8. Repair processes for confluent mouse cell cultures exposed to γ-rays at low LET.

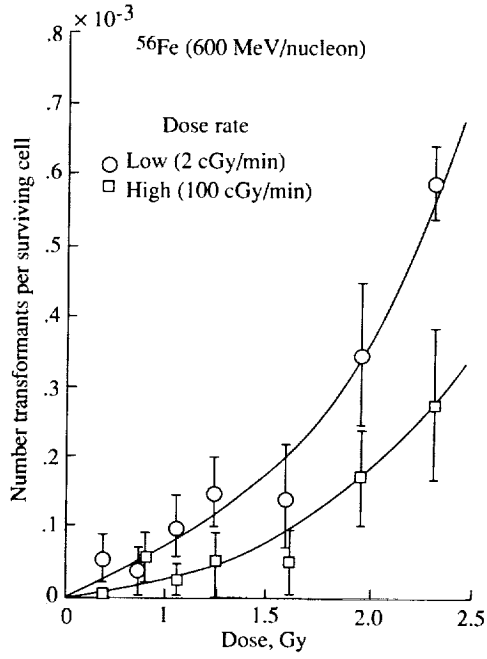

Figure 8.9. Cell transformation rate enhanced at low dose rate for high-LET exposure with possible misrepair mechanism indicated.

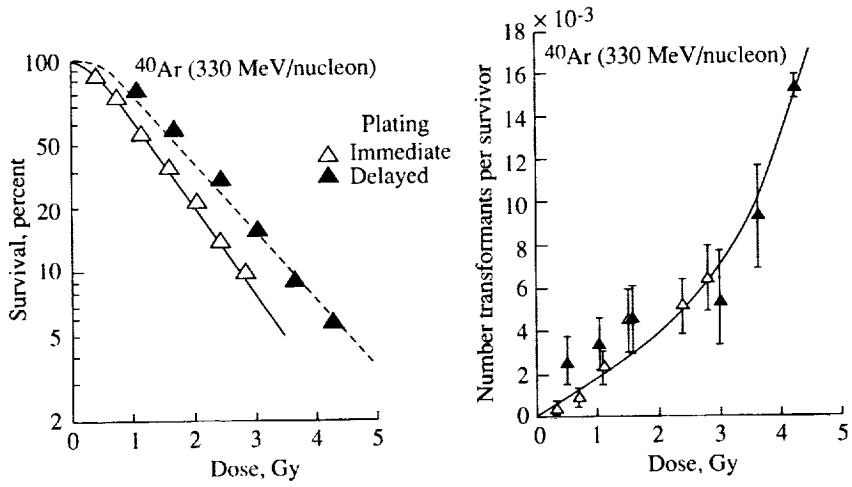

Figure 8.10. C3H10T1/2 cells irradiated by 330 MeV/u argon ions (Yang et al. 1986).

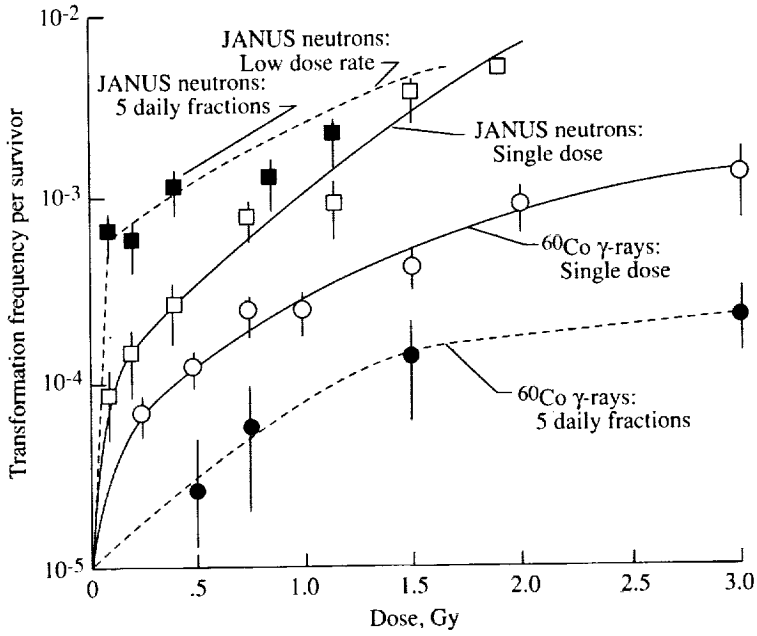

Figure 8.11. Transformation frequencies in C3H10T1/2 cells.

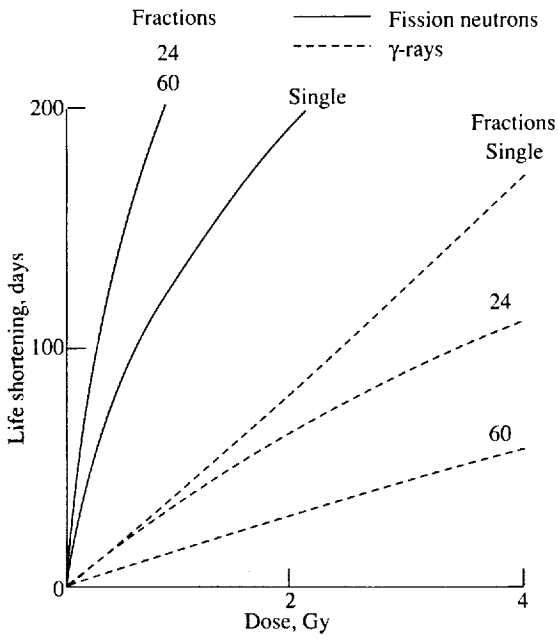

Figure 8.12. Life shortening in mice after single, 24, or 60 fractions of neutrons and after single, 24, or 60 fractions of γ-rays. Curves are fit to data of Thomson et al.

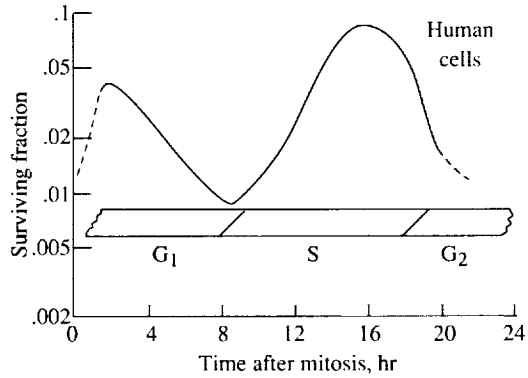

Figure 8.13. Survival of synchronized human cells exposed to 500 rads of 200 kV X-rays.

Clearly the risk to long-term GCR/SCR exposure will be difficult to evaluate because of the low dose rate, fractionated components, and the complex mixture of low- and high-LET radiations in space. Operative repair and cycle enhanced effects will require at least an intimate knowledge of the LET distributions at affected tissues or possibly more comprehensive track structure data.

8.4. Nuclear Models, Materials, and LET Spectra

As is clear from section 8.3, the distribution of exposure component over LET is a primary indicator of biological response. For example, low-LET components allow certain biological repairs at low dose rates and a low RBE value, whereas high-LET components can show increased biological effects at low dose rates and generally high RBE values. There is clear evidence that the relative contributions to exposure from various LET components can be altered through the choice of shield material. The transmitted LET spectrum for an aluminum shield is shown in figure 8.14, and the transmitted LET spectrum for a liquid hydrogen shield is shown in figure 8.15. Note that the LET spectra in figures 8.14 and 8.15 are for LET in the respective shield material. Although a rather large shift in LET can be accomplished by choice of shield composition, an exact evaluation must await improved nuclear fragmentation cross sections since uncertainty in cross sections cause LET shifts of the same order of magnitude. These shifts can be seen when the LET spectra in the Earth's atmosphere obtained by using the Bowman, Swiatecki, and Tsang (1973) fragmentation model shown in figure 8.16 are compared with the spectra obtained by using the Langley fragmentation model shown in figure 8.17.

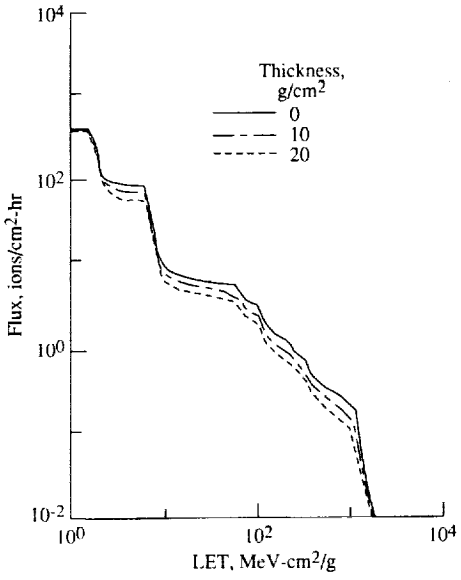

Figure 8.14. GCR integral LET spectra in aluminum for 30° orbit at altitude of 400 km.

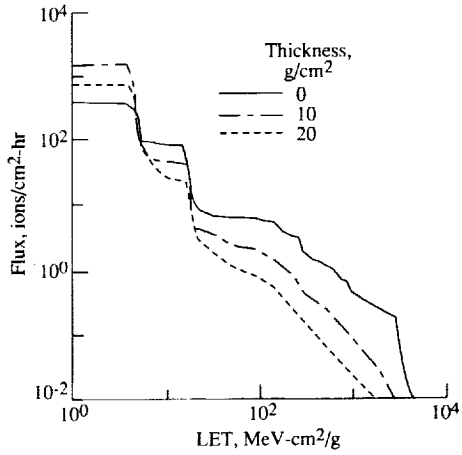

Figure 8.15. GCR integral LET spectra in hydrogen for 30° orbit at altitude of 400 km.

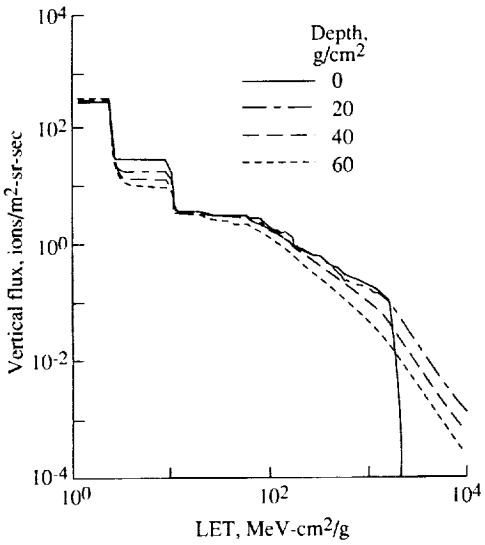

Figure 8.16. GCR integral LET spectra in Earth's atmosphere for fragmentation parameters of Bowman, Swiatecki, and Tsang (1973) model.

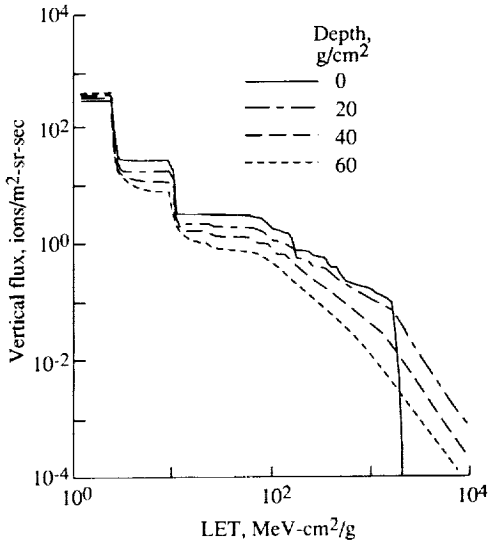

Figure 8.17. GCR integral LET spectra in Earth's atmosphere for fragmentation parameters of Langley Research Center model.

8.5. Human Geometry Factors

The significance of improving the accuracy (Shinn, Wilson, and Nealy 1990) for predicting the dose and dose equivalent that astronauts will incur during future NASA missions has been demonstrated in several studies (Townsend, Wilson, and Nealy 1988; Nealy, Wilson, and Townsend 1989). For example, Townsend, Wilson, and Nealy (1988) indicate that an increase of 20 percent in predicted BFO dose equivalent due to GCR's equates to a tripling of the required shield mass from 5 to 16 g/cm^2 of water to meet the recommended annual BFO limit of 0.5 Sv.

Large uncertainties are associated with the current dose estimate analysis, and every possible effort is needed to improve the accuracy to accomplish these missions in the most economical way without compromising the well-being of the astronauts.

One of the customary estimation practices (Beck, Stokes, and Lushbaugh 1972) that has been considered fairly reliable in the past is the use of the equivalent sphere model to obtain dose or dose equivalent to BFO. Langley and Billings (1972b) examined the feasibility of using a set of dosimetry spheres to monitor real-time organ doses received by astronauts under various space radiation and vehicle conditions. They made comparisons between the doses calculated for the spheres and the detailed body geometry under a range of solar proton energy spectrum characteristics and also under various vehicle radiation shielding thicknesses. The spectra were characterized by an assumed form described by Webber (1963). The optimal radii were determined for those spheres with the corresponding correlation constants that best represented the averaged organ doses under those assumed conditions. Although a moderate error of 18 percent for the correlation was found, one might question if the accuracy will hold under less idealized particle spectral conditions. This question was considered by Shinn, Wilson, and Nealy (1990) and we discuss those results herein.

The calculation made in a separate study (Simonsen et al. 1990) for the radiation transport through the atmosphere of Mars for the three largest solar flares observed in the last half century is extended here to include detailed BFO geometry. Comparisons are made for the dose equivalent to the various distributed BFO with the reported values based on the equivalent sphere model.

The Langley Research Center nucleon transport code BRYNTRN (Wilson et al. 1989b) was used by Simonsen et al. (1990) to obtain dose and dose equivalent on the surface of Mars caused by large solar flares. The transport code was based on the straight ahead approximation, which reduces consideration to one-dimensional transport; the merits of this approximation have been discussed elsewhere (Alsmiller et al. 1965; Alsmiller, Irving, and Moran 1968). An asymptotic expansion for the solution to the transport equation in two dimensions, subject to boundary conditions given for an arbitrary convex region, was derived by Wilson and Khandelwal (1974). The first term of the expansion was found to be an accurate approximation of the dose and for the case of an isotropic proton fluence spectrum is given by

$$D(\mathbf{x}) = 4\pi \int_0^\infty \phi(E) \int_0^\infty R(t, E)\ f_x(t)\ dt\ dE \tag{8.1}$$

with

$$\int_0^\infty f_x(t)\ dt = 1 \tag{8.2}$$

where $R(t, E)$ is the fluence-to-dose conversion factor at the depth t for normal incidence protons on a slab and $f_x(t)$ is the areal density distribution function for the point $\mathbf{x}$. The quantity $f_x(t)\ dt$ is the fraction of the solid angle for which the distance to the surface from the point $\mathbf{x}$ lies between t and $t + dt$.

To simplify the computational task (that is, without making any change to the BRYNTRN code), equation (8.1) is rewritten as

$$D(\mathbf{x}) = 4\pi \int_0^\infty f_x(t)\ D_x(t)\ dt \tag{8.3}$$

with

$$D_x(t) = \int_0^\infty \phi(E)\ R(t, E)\ dE \tag{8.4}$$

where $D_x(t)$ is the dose (or dose equivalent) at depth t for normal incidence protons on a slab of tissue. With the areal density distribution function for BFO given by the detailed geometry work described by Langley and Billings (1972a) and Billings and Yucker (1973), equation (8.3) can be calculated.

8.6. Results

The three solar flare spectra used for this study are those of February 1956, November 1960, and August 1972 events, whereas Langley and Billings used a Webber (1963) form of integral spectra given by the inverse exponential of proton magnetic rigidity with a range of rigidity parameter P_o from 50 to 200 MV. Figure 8.18 shows these three flare spectra and the best fit to the earlier two events with the Webber form. The actual spectra, especially the high-energy range of the February 1956 event (Foelsche et al. 1974), are different from the analytical form of Webber. The actual spectrum (Wilson and Denn 1976) for the August 1972 event is accurately approximated by the Webber form.

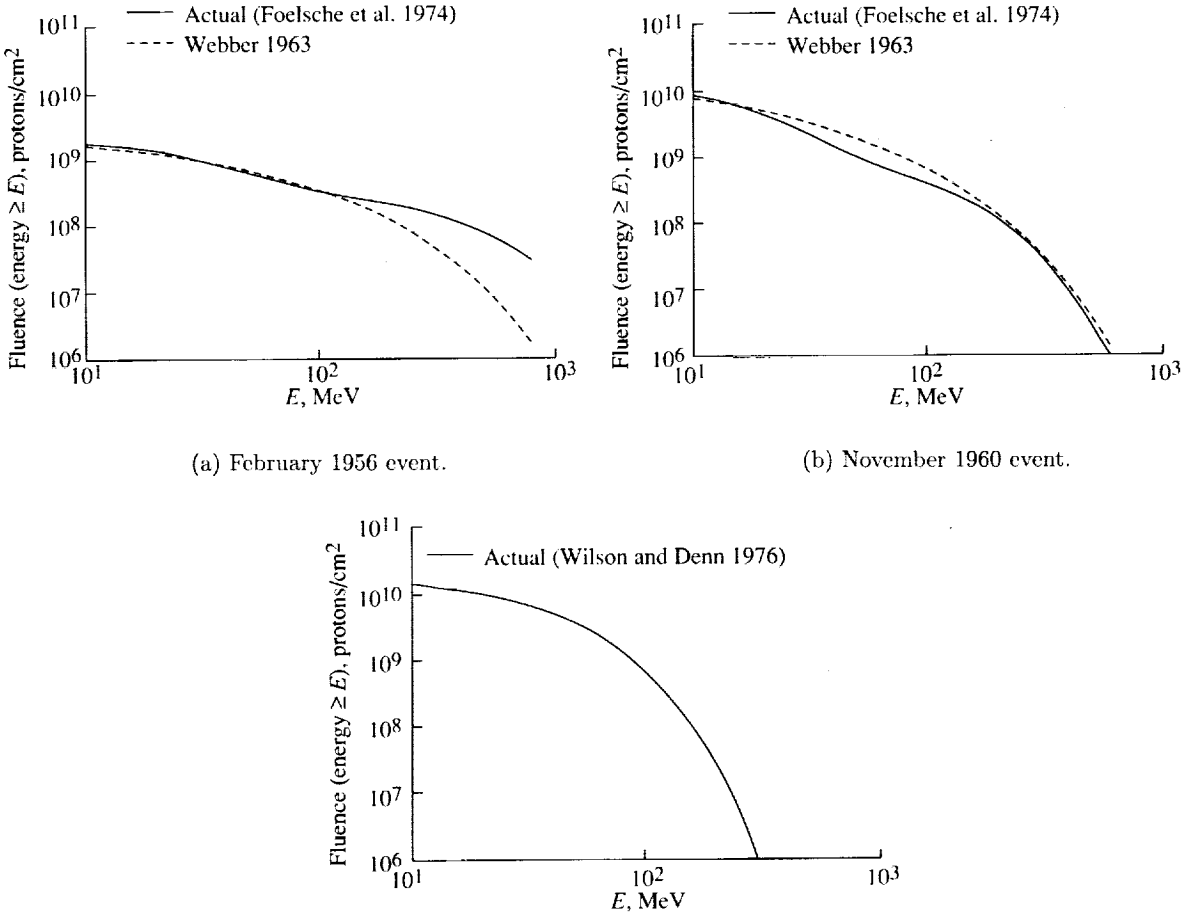

(a) February 1956 event.

(b) November 1960 event.

(c) August 1972 event. Webber spectrum fits actual event spectrum.

Figure 8.18. Fluence spectra for three major solar particle events.

The average dose equivalents at the surface of Mars caused by these three solar flare events are shown in figure 8.19 as a function of slab (water) thickness for the low-density Mars atmosphere model (16 g/cm^2 CO_2 vertically) used in Simonsen et al. (1990). These average dose equivalent values are obtained by summing the directional (anisotropic) dose equivalent over the solid angle and are used as $D_x(t)$ in this section. The calculated results from equation (8.3) are presented

in table 8.1 for the five distributed compartments of the blood-forming organs. Also shown for comparison are the average BFO and 5-cm (water) depth dose equivalents.

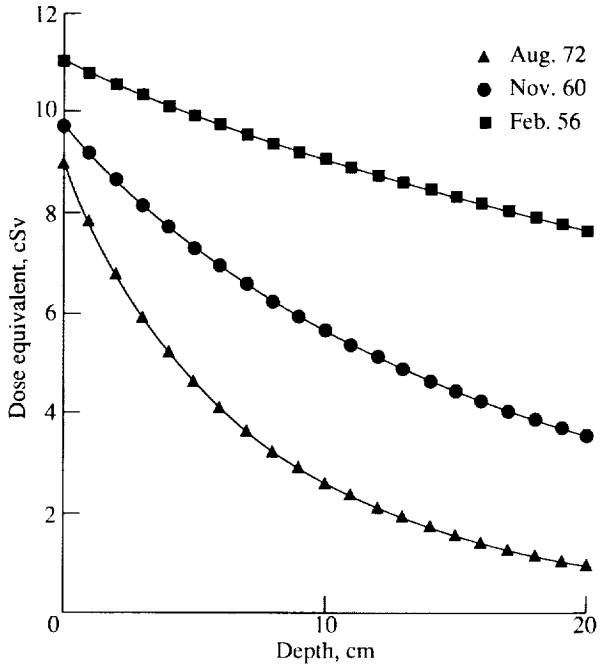

Figure 8.19. Dose equivalent at Mars surface as function of slab (water) thickness for low-density Mars atmosphere model.

It is customary (Space Science Board 1970; Beck, Stokes, and Lushbaugh 1972) to represent the average BFO exposure (dose or dose equivalent) with the 5-cm sphere based on the recommendation of the Space Science Board (1970). Conversely, the average BFO dose was found to be approximately half the 5-cm sphere dose in several analytical findings, such as the one from Langley and Billings (1972b). For the August 1972 event, the average BFO value for the detailed geometry (table 8.1) is fairly close (within 10 percent) to one half the value for a 5-cm sphere. However, the differences are larger for the other two flares, with 30 and 41 percent for November 1960 and February 1956 spectra, respectively. This wide discrepancy among these three events probably occurs because the two earlier flares contain more penetrating high-energy protons (fig. 8.18) and the actual spectra do not conform to the simple analytical form that Langley and Billings (1972b) used. We further note that the 5-cm sphere dose is conservative for these three events. Also, the 5-cm sphere dose is conservative as was found for GCR exposure by Townsend, Shinn, and Wilson (1991).

Table 8.1. BFO Dose Equivalent at Mars Surface for Low-Density Atmosphere Model

Solar flare event	Dose equivalent, cSv, for—						
	Arms	Legs	High trunk	Low trunk	Skull	Average BFO value	5-cm sphere
Feb. 1956	8.74	8.60	8.32	7.98	8.91	8.45	9.94
Nov. 1960	5.66	5.34	4.95	4.32	5.75	5.21	7.31
Aug. 1972	3.20	2.73	2.42	1.76	3.09	2.56	4.61

9. Concluding Remarks

Great progress has been made in developing codes for space shielding for future NASA programs. It is likewise clear that major uncertainties remain in the environmental model, the nuclear cross sections, and the methods for estimating biological risk. These uncertainties have an important impact on shield design and mission cost. Substantial work remains before all these issues can be resolved.

NASA Langley Research Center
Hampton, VA 23665-5225
November 8, 1991

10. References

Abramowitz, Milton; and Stegun, Irene A., eds. 1964: *Handbook of Mathematical Functions With Formulas, Graphs, and Mathematical Tables.* John Wiley & Sons, Inc. (Reprinted with corrections Dec. 1972.)

Adams, J. H., Jr.; Silberberg, R.; and Tsao, C. H. 1981: *Cosmic Ray Effects on Microelectronics. Part I– The Near-Earth Particle Environment.* NRL Memo. Rep. 4506–Pt. I, U.S. Navy. (Available from DTIC as AD A103 897.)

Adams, James H., Jr. 1987: *Cosmic Ray Effects on Microelectronics,* Part IV. NRL Memo. Rep. 5901 (Revised), Naval Research Lab.

Allkofer, O. C.; and Heinrich, W. 1974: Attenuation of Cosmic Ray Heavy Nuclei Fluxes in the Upper Atmosphere by Fragmentation. *Nuclear Phys.*, vol. B71, no. 3, pp. 429–438.

Alsmiller, R. G., Jr.; Irving, D. C.; Kinney, W. E.; and Moran, H. S. 1965: The Validity of the Straightahead Approximation in Space Vehicle Shielding Studies. *Second Symposium on Protection Against Radiations in Space,* Arthur Reetz, Jr., ed., NASA SP-71, pp. 177–181.

Alsmiller, R. G., Jr.; Irving, D. C.; and Moran, H. S. 1968: Validity of the Straightahead Approximation in Space-Vehicle Shielding Studies, Part II. *Nuclear Sci. & Eng.*, vol. 32, no. 1, pp. 56–61.

Anon. 1977: *Neutron Dosimetry for Biology and Medicine.* ICRU Rep. 26, International Commission on Radiation Units and Measurements.

Anon. 1986: *Mammography – A User's Guide, Recommendations of the National Council on Radiation Protection and Measurements.* NCRP Rep. No. 85.

Anon. 1989: *Guidance on Radiation Received in Space Activities.* NCRP Rep. No. 98, National Council on Radiation Protection and Measurements.

Beck, W. L.; Stokes, T. R.; and Lushbaugh, C. C. 1972: Dosimetry for Radiobiological Studies of the Human Hematopoietic System. *Proceedings of the National Symposium on Natural and Manmade Radiation in Space,* E. A. Warman, ed., NASA TM X-2440, pp. 974–981.

Benton, E. V.; Henke, R. P.; and Peterson, D. D. 1977: Plastic Nuclear Track Detector and Measurements of High-LET Particle Radiation on Apollo, Skylab, and ASTP Space Missions. *Nuclear Track Detect.*, vol. 1, no. 1, pp. 27–32.

Billings, M. P.; and Yucker, W. R. 1973: *The Computerized Anatomical Man (CAM) Model.* NASA CR-134043.

Bowman, J. D.; Swiatecki, W. J.; and Tsang, C. F. 1973: *Abrasion and Ablation of Heavy Ions.* LBL-2908, Lawrence Berkeley Lab., Univ. of California.

Brenner, D. J.; and Hall, E. J. 1990: The Inverse Dose-Rate Effect for Oncogenic Transformation by Neutrons and Charged Particles: A Plausible Interpretation Consistent With Published Data. *Int. J. Radiat. & Biol.*, vol. 58, no. 5, pp. 745–758.

Chatterjee, A.; Tobias, C. A.; and Lyman, J. T. 1976: Nuclear Fragmentation in Therapeutic and Diagnostic Studies With Heavy Ions. *Spallation Nuclear Reactions and Their Applications,* B. S. P. Shen and M. Merker, eds., D. Reidel Publ. Co., pp. 169–191.

Cleghorn, T. F.; Freier, P. S.; and Waddington, C. J. 1968: The Energy Dependence of the Fragmentation Parameters and Mean Free Paths of Cosmic-Ray Nuclei With $Z \geq 10$. *Canadian J. Phys.*, vol. 46, no. 10, pp. S572–S577.

Cucinotta, Francis A.; Katz, Robert; Wilson, John W.; Townsend, Lawrence W.; Nealy, John E.; and Shinn, Judy L. 1991: *Cellular Track Model of Biological Damage to Mammalian Cell Cultures From Galactic Cosmic Rays.* NASA TP-3055.

Curtis, S. B.; Doherty, W. R.; and Wilkinson, M. C. 1969: *Study of Radiation Hazards to Man on Extended Near Earth Missions.* NASA CR-1469.

Curtis, S. B.; and Wilkinson, M. C. 1972: The Heavy Particle Hazard What Physical Data Are Needed? *Proceedings of the National Symposium on Natural and Manmade Radiation in Space,* E. A. Warman, ed., NASA TM X-2440, pp. 1007 1015.

Curtis, Stanley B. 1986: Lethal and Potentially Lethal Lesions Induced by Radiation—A Unified Repair Model. *Radiat. Res.*, vol. 106, pp. 252–270.

Davis, Leverett, Jr. 1960: On the Diffusion of Cosmic Rays in the Galaxy. *Proceedings of the Moscow Cosmic Ray Conference,* International Union of Pure and Applied Physics (Moscow), pp. 220–225.

Elkind, M. M.; and Sutton, Harriet 1960: Radiation Response of Mammalian Cells Grown in Culture. I. Repair of X-Ray Damage in Surviving Chinese Hamster Cells. *Radiat. Res.*, vol. 13, nos. 1 6, pp. 556 593.

Feshbach, H.; and Huang, K. 1973: Fragmentation of Relativistic Heavy Ions. *Phys. Lett.,* vol. 47B, no. 4, pp. 300–302.

Foelsche, Trutz; Mendell, Rosalind B.; Wilson, John W.; and Adams, Richard R. 1974: *Measured and Calculated Neutron Spectra and Dose Equivalent Rates at High Altitudes; Relevance to SST Operations and Space Research.* NASA TN D-7715.

Fritz-Niggli, Hedi 1988: The Role of Repair Processes in Cellular and Genetical Response to Radiation. *Terrestrial Space Radiation and Its Biological Effects,* Percival D. McCormack, Charles E. Swenberg, and Horst Bücker, eds., Plenum Press, pp. 213–235.

Ganapol, Barry D.; Townsend, Lawrence W.; and Wilson, John W. 1989: *Benchmark Solutions for the Galactic Ion Transport Equations: Energy and Spatially Dependent Problems.* NASA TP-2878.

Ginzburg, V. L.; and Syrovatskii, S. I. (H. S. H. Massey, transl., and D. Ter Haar, ed.) 1964: *The Origin of Cosmic Rays.* Macmillan Co.

Gloeckler, G.; and Jokipii, J. R. 1969: Physical Basis of the Transport and Composition of Cosmic Rays in the Galaxy. *Phys. Review Lett.*, vol. 22, no. 26, pp. 1448–1453.

Goldhaber, A. S. 1974: Statistical Models of Fragmentation Processes. *Phys. Lett.*, vol. 53B, no. 4, pp. 306 308.

Gosset, J.; Gutbrod, H. H; Meyer, W. G.; Poskanzer, A. M.; Sandoval, A.; Stock, R.; and Westfall, G. D. 1977: Central Collisions of Relativistic Heavy Ions. *Phys. Review,* vol. 16, ser. C, no. 2, pp. 629 657.

Guerreau, D.; Borrel, V.; Jacquet, D.; Galin, J.; Gatty, B.; and Tarrago, X. 1983: Isotopic Distributions of Projectile-Like Fragments in 44 MeV/u ^{40}Ar Induced Reactions. *Phys. Lett.*, vol. 131B, no. 4, 5, 6, pp. 293 296.

Guthrie, Miriam P. 1970: EVAP-4: *Another Modification of a Code To Calculate Particle Evaporation From Excited Compound Nuclei.* ORNL-TM-3119, U.S. Atomic Energy Commission.

Heckman, H. H.; Greiner, D. E.; Lindstrom, P. J.; and Bieser, F. S. 1972: Fragmentation of ^{14}N Nuclei at 29 GeV: Inclusive Isotope Spectra at 0°. *Phys. Review Lett.,* vol. 28, no. 14, pp. 926–929.

Heckman, H. H. 1975: *Heavy Ion Fragmentation Experiments at the Bevatron.* NASA CR-142589.

Hill, C. K.; Buonaguro, F. M.; Myers, C. P.; Han, A.; and Elkind, M. M. 1982: Fission-Spectrum Neutrons at Reduced Dose Rates Enhance Neoplastic Transformation. *Nature,* vol. 298, pp. 67 69.

Hill, C. K.; Carnes, B. A.; Han, A.; and Elkind, M. M. 1985: Neoplastic Transformation Is Enhanced by Multiple Low Doses of Fission-Spectrum Neutrons. *Radiat. Res.,* vol. 102, pp. 404 410.

Hüfner, J.; Schäfer, K.; and Schürmann, B. 1975: Abrasion-Ablation in Reactions Between Relativistic Heavy Ions. *Phys. Review,* vol. 12, ser. C, no. 6, pp. 1888–1898.

Krebs, A. T. 1950: Possibility of Biological Effects of Cosmic Rays in High Altitudes, Stratosphere and Space. *J. Aviation Med.,* vol. 21, no. 6, pp. 481–494.

Kovalev, E. E.; Muratova, I. A.; and Petrov, V. M. 1989: Studies of the Radiation Environment Aboard Prognoz Satellites. *Nuclear Tracks Radiat. Meas.*, vol. 14, no. 1, pp. 45–48.

Khandelwal, G. S.; and Wilson, John W. 1974: *Proton Tissue Dose for the Blood Forming Organ in Human Geometry: Isotropic Radiation.* NASA TM X-3089.

Langley, R. W.; and Billings, M. P. 1972a: Methods of Space Radiation Dose Analysis With Applications to Manned Space Systems. *Proceedings of the National Symposium on Natural and Manmade Radiation in Space,* E. A. Warman, ed., NASA TM X-2440, pp. 108–116.

Langley, R. W.; and Billings, M. P. 1972b: A New Model for Estimating Space Proton Dose to Body Organs. *Nuclear Technol.*, vol. 15, no. 1, pp. 68 74.

Letaw, John; Tsao, C. H.; and Silberberg, R. 1983: Matrix Methods of Cosmic Ray Propagation. *Composition and Origins of Cosmic Rays,* Maurice M. Shapiro, ed., D. Reidel Publ. Co., pp. 337 342.

Lezniak, J. A. 1979: The Extension of the Concept of the Cosmic-Ray Path-Length Distribution to Nonrelativistic Energies. *Astrophys. & Space Sci.,* vol. 63, no. 2, pp. 279 293.

Morrissey, D. J.; Marsh, W. R.; Otto, R. J.; Loveland, W.; and Seaborg, G. T. 1978: Target Residue Mass and Charge Distributions in Relativistic Heavy Ion Reactions. *Phys. Review,* vol. 18, ser. C, no. 3, pp. 1267 1274.

Nachtwey, D. Stuart; and Yang, Tracy Chui-Hsu 1991: Radiological Health Risks for Exploratory Class Missions in Space. *Acta Astronaut.,* vol. 23, pp. 227 231.

Nealy, John E.; Wilson, John W.; and Townsend, Lawrence W. 1989: Preliminary Analyses of Space Radiation Protection for Lunar Base Surface Systems. SAE Tech. Paper Ser. 891487.

Nealy, John E.; Simonsen, Lisa C.; Townsend, Lawrence W.; and Wilson, John W. 1990: Deep-Space Radiation Exposure Analysis for Solar Cycle XXI (1975 1986). SAE Tech. Paper Ser. 901347.

Norbury, John W.; and Townsend, Lawrence W. 1986: *Electromagnetic Dissociation Effects in Galactic Heavy-Ion Fragmentation.* NASA TP-2527.

Peters, B. 1958: The Nature of Primary Cosmic Radiation. *Progress in Cosmic Ray Physics,* J. G. Wilson, ed., Interscience Publ., Inc., pp. 191 242.

Raisbeck, G. M.; and Yiou, F. 1975: Production Cross Sections of Be Isotopes in C and O Targets Bombarded by 2.8-GeV α Particles: Implications for Factorization. *Phys. Review Lett.,* vol. 35, no. 3, pp. 155–159.

Rossi, H. H.; and Kellerer, A. M. 1986: The Dose Rate Dependence of Oncogenic Transformation by Neutrons May Be Due to Variation of Response During the Cell Cycle. *Int. J. Radiat. & Biol.*, vol. 50, no. 2, pp. 353 361.

Rudstam, G. 1966: Systematics of Spallation Yields. *Zeitschrift fur Naturforschung,* vol. 21a, no. 7, pp. 1027 1041.

Schimmerling, Walter; Miller, Jack; Wong, Mervyn; Rapkin, Marwin; Howard, Jerry; Spieler, Helmut G.; and Jarret, Blair V. 1989: The Fragmentation of 670A MeV Neon-20 as a Function of Depth in Water. *Radiat. Res.*, vol. 120, pp. 36 71.

Schimmerling, Walter 1990: Ground-Based Measurements of Galactic Cosmic Ray Fragmentation in Shielding. Paper presented at the 28th Plenary Meeting of COSPAR (The Hague, The Netherlands).

Shinn, Judy L.; Wilson, John W.; and Nealy, John E. 1990: *Reliability of Equivalent Sphere Model in Blood-Forming Organ Dose Estimation.* NASA TM-4178.

Silberberg, R.; Tsao, C. H.; and Shapiro, M. M. 1976: Semiempirical Cross Sections, and Applications to Nuclear Interactions of Cosmic Rays. *Spallation Nuclear Reactions and Their Applications,* B. S. P. Shen and M. Merker, eds., D. Reidel Publ. Co., pp. 49 81.

Silberberg, R.; Tsao, C. H.; and Letaw, John R. 1983: Improvement of Calculations of Cross Sections and Cosmic-Ray Propagation. *Composition and Origin of Cosmic Rays,* Maurice M. Shapiro, ed., D. Reidel Publ. Co., pp. 321–336.

Simonsen, Lisa C.; Nealy, John E.; Townsend, Lawrence W.; and Wilson, John W. 1990: *Radiation Exposure for Manned Mars Surface Missions.* NASA TP-2979.

Space Science Board 1970: *Radiation Protection Guides and Constraints for Space-Mission and Vehicle-Design Studies Involving Nuclear Systems.* National Academy of Sciences—National Research Council.

Swenberg, Charles E.; Holwitt, Eric A.; and Speicher, James M. 1990: Superhelicity and DNA Radiation Sensitivity. SAE Tech. Paper Ser. 901349.

Terasima, Toyozo; and Tolmach, L. J. 1963: Variations in Several Responses of HeLa Cells to X-Irradiation During the Division Cycle. *Biophys. J.*, vol. 3, no. 1, pp. 11 33.

Thomson, John F.; Williamson, Frank S.; Grahn, Douglas; and Ainsworth, E. John 1981a: Life Shortening in Mice Exposed to Fission Neutrons and γ Rays. I. Single and Short-Term Fractionated Exposures. *Radiat. Res.*, vol. 86, pp. 559 572.

Thomson, John F.; Williamson, Frank S.; Grahn, Douglas; and Ainsworth, E. John 1981b: Life Shortening in Mice Exposed to Fission Neutrons and γ Rays. II. Duration-of-Life and Long-Term Fractionated Exposures. *Radiat. Res.*, vol. 86, pp. 573–579.

Thomson, John F.; Williamson, Frank S.; and Grahn, D. 1983: Life Shortening in Mice Exposed to Fission Neutrons and γ Rays. III. Neutron Exposures of 5 and 10 Rad. *Radiat. Res.*, vol. 93, pp. 205 209.

Thomson, John F.; Williamson, Frank S.; and Grahn, Douglas 1985a: Life Shortening in Mice Exposed to Fission Neutrons and γ Rays. IV. Further Studies With Fractionated Neutron Exposures. *Radiat. Res.*, vol. 103, pp. 77–88.

Thomson, John F.; Williamson, Frank S.; and Grahn, Douglas 1985b: Life Shortening in Mice Exposed to Fission Neutrons and γ Rays. V. Further Studies With Single Low Doses. *Radiat. Res.*, vol. 104, pp. 420 428.

Thomson, John F.; Williamson, Frank S.; and Grahn, Douglas 1986: Life Shortening in Mice Exposed to Fission Neutrons and γ Rays. VI. Studies With the White-Footed Mouse, Peromyscus Leucopus. *Radiat. Res.*, vol. 108, pp. 176 188.

Thomson, John F.; and Grahn, Douglas 1988: Life Shortening in Mice Exposed to Fission Neutrons and γ Rays. VII. Effects of 60 Once-Weekly Exposures. *Radiat. Res.*, vol. 115, pp. 347 360.

Thomson, John F.; and Grahn, Douglas 1989: Life Shortening in Mice Exposed to Fission Neutrons and γ Rays. VIII. Exposures to Continuous γ Radiation. *Radiat. Res.*, vol. 118, pp. 151 160.

Todd, Paul; and Tobias, Cornelius A. 1974: Cellular Radiation Biology. *Space Radiation Biology and Related Topics,* Cornelius A. Tobias and Paul Todd, eds., Academic Press, Inc., pp. 141 196.

Townsend, Lawrence W.; Wilson, John W.; Norbury, John W.; and Bidasaria, Hari B. 1984: *An Abrasion-Ablation Model Description of Galactic Heavy-Ion Fragmentation.* NASA TP-2305.

Townsend, L. W.; Wilson, J. W.; and Norbury, J. W. 1985: A Simplified Optical Model Description of Heavy Ion Fragmentation. *Canadian J. Phys.*, vol. 63, no. 2, pp. 135–138.

Townsend, L. W.; Wilson, J. W.; Cucinotta, F. A.; and Norbury, J. W. 1986a: Comparison of Abrasion Model Differences in Heavy Ion Fragmentation: Optical Versus Geometric Models. *Phys. Review,* vol. 34, ser. C, no. 4, pp. 1491 1494.

Townsend, Lawrence W.; Wilson, John W.; Cucinotta, Francis A.; and Norbury, John W. 1986b: *Optical Model Calculations of Heavy-Ion Target Fragmentation.* NASA TM-87692.

Townsend, L. W.; and Wilson, J. W. 1988: An Evaluation of Energy-Independent Heavy Ion Transport Coefficient Approximations. *Health Phys.*, vol. 54, no. 4, pp. 409–412.

Townsend, Lawrence W.; Wilson, John W.; and Nealy, John E. 1988: *Preliminary Estimates of Galactic Cosmic Ray Shielding Requirements for Manned Interplanetary Missions.* NASA TM-101516.

Townsend, Lawrence W.; Ganapol, Barry D.; and Wilson, John W. 1989: Benchmark Solutions for Heavy Ion Transport Code Validation. *Abstracts of Papers for the Thirty-Seventh Annual Meeting of the Radiation Research Society and Ninth Annual Meeting of the North American Hyperthermia Group,* Radiation Research Soc., p. 126.

Townsend, Lawrence W.; Wilson, John W.; and Nealy, John E. 1989: Space Radiation Shielding Strategies and Requirements for Deep Space Missions. SAE Tech. Paper Ser. 891433.

Townsend, Lawrence W.; Shinn, Judy L.; and Wilson, John W. 1991: Interplanetary Crew Exposure Estimates for the August 1972 and October 1989 Solar Particle Events. *Radiat. Res.*, vol. 126, pp. 108 110.

Viyogi, Y. P.; Symons, T. J. M.; Doll, P.; Greiner, D. E.; Heckman, H. H.; Hendrie, D. L.; Lindstrom, P. J.; Mahoney, J.; Scott, D. K.; Van Bibber, K.; Westfall, G. D.; Wieman, H.; Crawford, H. J.; McParland, C.; and Gelbke, C. K. 1979: Fragmentations of ^{40}Ar at 213 MeV/Nucleon. *Phys. Review Lett.*, vol. 42, no. 1, pp. 33 36.

Webber, W. R. 1963: *An Evaluation of the Radiation Hazard Due to Solar-Particle Events.* D2-90469, Aero-Space Div., Boeing Co.

Webber, W. R.; Brautigam, D. A.; Kish, J. C.; and Schrier, D. A. 1983a: Fragmentation of ~500 MeV/nuc Ne and O Nuclei in CH_2, C and H Targets —Charge and Isotopic Cross Sections. *18th International Cosmic Ray Conference Conference Papers,* OG Sessions, Vol. 2, Tata Inst. of Fundamental Research (Colaba, Bombay), pp. 202–205.

Webber, W. R.; Brautigam, D. A.; Kish, J. C.; and Schrier, D. A. 1983b: Fragmentation of 710 and 1050 MeV/nuc Fe Nuclei in CH_2 and C Targets Isotopic Cross Sections for H Targets. *18th International Cosmic Ray Conference Conference Papers,* OG Sessions, Vol. 2, Tata Inst. of Fundamental Research (Colaba, Bombay), pp. 198 201.

Westfall, G. D.; Wilson, Lance W.; Lindstrom, P. J.; Crawford, H. J.; Greiner, D. E.; and Heckman, H. H. 1979: Fragmentation of Relativistic ^{56}Fe. *Phys. Review,* vol. 19, ser. C, no. 4, pp. 1309 1323.

Wilson, John W.; and Khandelwal, G. S. 1974: Proton Dose Approximation in Arbitrary Convex Geometry. *Nuclear Technol.*, vol. 23, no. 3, pp. 298–305.

Wilson, John W.; and Lamkin, Stanley L. 1975: Perturbation Theory for Charged-Particle Transport in One Dimension. *Nuclear Sci. & Eng.*, vol. 57, no. 4, Aug. 1975, pp. 292–299.

Wilson, John W.; and Denn, Fred M. 1976: *Preliminary Analysis of the Implications of Natural Radiations on Geostationary Operations.* NASA TN D-8290.

Wilson, John W. 1977a: *Analysis of the Theory of High-Energy Ion Transport.* NASA TN D-8381.

Wilson, J. W. 1977b: Depth-Dose Relations for Heavy Ion Beams. *Virginia J. Sci.*, vol. 28, no. 3, pp. 136 138.

Wilson, J. W.; and Townsend, L. W. 1981: An Optical Model for Composite Nuclear Scattering. *Canadian J. Phys.*, vol. 59, no. 11, pp. 1569 1576.

Wilson, John W. 1983: *Heavy Ion Transport in the Straight Ahead Approximation.* NASA TP-2178.

Wilson, John W.; Townsend, L. W.; Bidasaria, H. B.; Schimmerling, Walter; Wong, Mervyn; and Howard, Jerry 1984: ^{20}Ne Depth-Dose Relations in Water. *Health Phys.*, vol. 46, no. 5, pp. 1101 1111.

Wilson, John W.; and Badavi, F. F. 1986: Methods of Galactic Heavy Ion Transport. *Radiat. Res.*, vol. 108, pp. 231–237.

Wilson, J. W.; Townsend, L. W.; and Badavi, F. F. 1987a: Galactic HZE Propagation Through the Earth's Atmosphere. *Radiat. Res.*, vol. 109, no. 2, pp. 173 183.

Wilson, John W.; Townsend, Lawrence W.; and Badavi, F. F. 1987b: A Semiempirical Nuclear Fragmentation Model. *Nuclear Instrum. & Methods Phys. Res.*, vol. B18, no. 3, pp. 225–231.

Wilson, John W.; and Townsend, L. W. 1988: A Benchmark for Galactic Cosmic-Ray Transport Codes. *Radiat. Res.*, vol. 114, no. 2, pp. 201 206.

Wilson, John W.; Townsend, Lawrence W.; Ganapol, Barry; Chun, Sang Y.; and Buck, Warren W. 1988: Charged-Particle Transport in One Dimension. *Nuclear Sci. & Eng.*, vol. 99, no. 3, pp. 285 287.

Wilson, John W.; Lamkin, Stanley L.; Farhat, Hamidullah; Ganapol, Barry D.; and Townsend, Lawrence W. 1989a: *A Hierarchy of Transport Approximations for High Energy Heavy (HZE) Ions.* NASA TM-4118.

Wilson, John W.; Townsend, Lawrence W.; Nealy, John E.; Chun, Sang Y.; Hong, B. S.; Buck, Warren W.; Lamkin, S. L.; Ganapol, Barry D.; Khan, Ferdous; and Cucinotta, Francis A. 1989b: BRYNTRN: *A Baryon Transport Model.* NASA TP-2887.

Wilson, J. W.; Townsend, L. W.; Lamkin, S. L.; and Ganapol, B. D. 1990: A Closed-Form Solution to HZE Propagation. *Radiat. Res.*, vol. 122, no. 3, pp. 223 228.

Wilson, John W.; Townsend, Lawrence W.; Schimmerling, Walter; Khandelwal, Govind S.; Khan, Ferdous; Nealy, John E.; Cucinotta, Francis A.; Simonsen, Lisa C.; Shinn, Judy L.; and Norbury, John W. 1991: *Transport Methods and Interactions for Space Radiations.* NASA RP-1257.

Yang, Tracy Chui-Hsu; Craise, Laurie M.; Mei, Man-Tong; and Tobias, Cornelius A. 1986: Dose Protraction Studies With Low- and High-LET Radiations on Neoplastic Cell Transformation In Vitro. *Adv. Space Res.*, vol. 6, no. 11, pp. 137–147.

Yang, Tracy Chui-Hsu; Craise, Laurie M.; Mei, Man-Tong; and Tobias, Cornelius A. 1989: Neoplastic Cell Transformation by High-LET Radiation: Molecular Mechanisms. *Adv. Space Res.*, vol. 9, no. 10, pp. 131–140.

REPORT DOCUMENTATION PAGE

Form Approved
OMB No. 0704-0188

1. AGENCY USE ONLY *(Leave blank)*	2. REPORT DATE	3. REPORT TYPE AND DATES COVERED
	December 1991	Technical Paper

4. TITLE AND SUBTITLE
HZETRN: A Heavy Ion/Nucleon Transport Code for Space Radiations

5. FUNDING NUMBERS
WU 593-42-11-01

6. AUTHOR(S)
John W. Wilson, Sang Y. Chun, Forooz F. Badavi,
Lawrence W. Townsend, and Stanley L. Lamkin

7. PERFORMING ORGANIZATION NAME(S) AND ADDRESS(ES)
NASA Langley Research Center
Hampton, VA 23665-5225

8. PERFORMING ORGANIZATION REPORT NUMBER
L-16952

9. SPONSORING/MONITORING AGENCY NAME(S) AND ADDRESS(ES)
National Aeronautics and Space Administration
Washington, DC 20546-0001

10. SPONSORING/MONITORING AGENCY REPORT NUMBER
NASA TP-3146

11. SUPPLEMENTARY NOTES
Wilson and Townsend: Langley Research Center, Hampton, VA; Chun and Badavi: Old Dominion University, Norfolk, VA; Lamkin: Analytical Services & Materials, Inc., Hampton, VA.

12a. DISTRIBUTION/AVAILABILITY STATEMENT
Unclassified Unlimited

Subject Category 93

12b. DISTRIBUTION CODE

13. ABSTRACT *(Maximum 200 words)*
The galactic heavy ion transport code (GCRTRN) and the nucleon transport code (BRYNTRN) are integrated into a code package (HZETRN). The code package is computer efficient and capable of operating in an engineering design environment for manned deep space mission studies. The nuclear data set used by the code is discussed including current limitations. Although the heavy ion nuclear cross sections are assumed constant, the nucleon-nuclear cross sections of BRYNTRN with full energy dependence are used. The relation of the final code to the Boltzmann equation is discussed in the context of simplifying assumptions. Error generation and propagation is discussed, and comparison is made with simplified analytic solutions to test numerical accuracy of the final result. A brief discussion of biological issues and their impact on fundamental developments in shielding technology is given.

14. SUBJECT TERMS	15. NUMBER OF PAGES
Ion transport; Radiation protection; Shielding materials	45
	16. PRICE CODE: A03

17. SECURITY CLASSIFICATION OF REPORT	18. SECURITY CLASSIFICATION OF THIS PAGE	19. SECURITY CLASSIFICATION OF ABSTRACT	20. LIMITATION OF ABSTRACT
Unclassified	Unclassified		